เอสเทอริฟิเคชันแบบเลือกจำเพาะของกลีเซอรอลกับกรดโอเลอิกโดยใช้กรดทังสโตฟอสฟอริกรองรับด้วยมีโซพอรัสซิลิกาที่เติมหมู่ฟังก์ชัน

นางสาวกุลธิดา รัชฎาภิบาล

วิทยานิพนธ์นี้เป็นส่วนหนึ่งของการศึกษาตามหลักสูตรปริญญาวิทยาศาสตรมหาบัณฑิต
สาขาวิชาเคมี ภาควิชาเคมี
คณะวิทยาศาสตร์ จุฬาลงกรณ์มหาวิทยาลัย
ปีการศึกษา 2560

SELECTIVE ESTERIFICATION OF GLYCEROL WITH OLEIC ACID USING TUNGSTOPHOSPHORIC ACID SUPPORTED ON FUNCTIONALIZED MESOPOROUS SILICA

Miss Kullatida Ratchadapiban

A Thesis Submitted in Partial Fulfillment of the Requirements
for the Degree of Master of Science Program in Chemistry
Department of Chemistry
Faculty of Science
Chulalongkorn University
Academic Year 2017

Thesis Title	SELECTIVE ESTERIFICATION OF GLYCEROL WITH OLEIC ACID USING TUNGSTOPHOSPHORIC ACID SUPPORTED ON FUNCTIONALIZED MESOPOROUS SILICA
By	Miss Kullatida Ratchadapiban
Field of Study	Chemistry
Thesis Advisor	Wipark Anutrasakda, Ph.D.
Thesis Co-Advisor	Duangamol Tungasmita, Ph.D.

Accepted by the Faculty of Science, Chulalongkorn University in Partial Fulfillment of the Requirements for the Master's Degree

.....Dean of the Faculty of Science
(Associate Professor Polkit Sangvanich, Ph.D.)

THESIS COMMITTEE

.....Chairman
(Associate Professor Vudhichai Parasuk, Ph.D.)

.....Thesis Advisor
(Wipark Anutrasakda, Ph.D.)

.....Thesis Co-Advisor
(Duangamol Tungasmita, Ph.D.)

.....Examiner
(Numpon Insin, Ph.D.)

.....External Examiner
(Kittisak Choojun, Ph.D.)

กุลธิดา รัชฎาภิบาล : เอสเทอริฟิเคชันแบบเลือกจำเพาะของกลีเซอรอลกับกรดโอเลอิกโดยใช้กรดทังสโตฟอสฟอริกรองรับด้วยมีโซพอรัสซิลิกาที่เติมหมู่ฟังก์ชัน (SELECTIVE ESTERIFICATION OF GLYCEROL WITH OLEIC ACID USING TUNGSTOPHOSPHORIC ACID SUPPORTED ON FUNCTIONALIZED MESOPOROUS SILICA) อ.ที่ปรึกษาวิทยานิพนธ์หลัก: อ. ดร.วิภาค อนุตรศักดา, อ.ที่ปรึกษาวิทยานิพนธ์ร่วม: อ. ดร.ดวงกมล ตุงคะสมิต, 87 หน้า.

ในงานวิจัยนี้ กลุ่มของวัสดุเมโซพอรัสซิลิกาชนิดเอสบีเอ 15 ที่ถูกเติมหมู่ฟังก์ชันเอมีนแล้วทำให้เป็นกรดถูกสังเคราะห์ขึ้นสำเร็จ โดยวัสดุเมโซพอรัสซิลิกาชนิดเอสบีเอ 15 ถูกเติมหมู่ฟังก์ชันด้วยสารประกอบไซเลนที่มีหมู่ฟังก์ชันเอมีนสามชนิด คือ APTES (N) AAPTMS (NN) และ DETTMS (NNN) จากนั้นวัสดุหลังเติมหมู่ฟังก์ชันถูกทำให้เป็นกรดด้วยกรดทังสโตฟอสฟอริกซึ่งมีโครงสร้างแบบเคกกิ้นที่สองความเข้มข้นคือร้อยละ 20 โดยน้ำหนัก (H20) และร้อยละ 40 โดยน้ำหนัก (H40) วัสดุที่สังเคราะห์ได้ทั้งหกชนิดจะถูกเรียกแทนด้วย S-N1-H20 S-N1-H40 S-NN1-H20 S-NN1-H40 S-NNN1-H20 และ S-NNN1-H40 วัสดุเหล่านี้ได้รับการพิสูจน์เอกลักษณ์ด้วยเทคนิคการเลี้ยวเบนของรังสีเอกซ์ เทคนิคการตรวจวัดพื้นที่ผิวและความมีรูพรุน เทคนิคอินฟราเรด กล้องจุลทรรศน์แบบส่องกราดที่เชื่อมต่อกับอุปกรณ์วิเคราะห์ธาตุเชิงพลังงาน กล้องจุลทรรศน์แบบส่องผ่าน และเทคนิคการวิเคราะห์หาองค์ประกอบธาตุ ผลการวิเคราะห์พบว่าวัสดุที่สังเคราะห์ได้ยังคงมีความเป็นรูพรุนแบบเมโซชนิดหกเหลี่ยมค่อนข้างสูงและลักษณะภายนอกของวัสดุมีรูปร่างคล้ายเกลียวเชือก บ่งชี้ได้ว่าโครงสร้างหลักของวัสดุรองรับเอสบีเอ 15 ยังคงถูกรักษาไว้ภายหลังการดัดแปรพื้นผิวด้วยสารประกอบไซเลนที่มีหมู่ฟังก์ชันเอมีน และกรดทังสโตฟอสฟอริก วัสดุที่สังเคราะห์ได้มีพื้นที่ผิว ขนาดเส้นผ่านศูนย์กลางของรูพรุน และความเป็นกรดอยู่ในช่วง 55 ถึง 299 ตารางเมตรต่อกรัม 6.18 ถึง 7.05 นาโนเมตร และ 0.18 ถึง 0.49 มิลลิโมลต่อกรัม ตามลำดับ

วัสดุที่สังเคราะห์ได้ถูกทดสอบการเป็นตัวเร่งปฏิกิริยาสำหรับปฏิกิริยาเอสเทอริฟิเคชันของกลีเซอรอลกับกรดโอเลอิกเพื่อสังเคราะห์มอนอโอเลอินโดยใช้กลีเซอรอลต่อกรดโอเลอิกในอัตราส่วน 4 ต่อ 1 โดยโมลที่อุณหภูมิ 160 องศาเซลเซียสเป็นเวลา 3 ชั่วโมงและเติมตัวเร่งปฏิกิริยาร้อยละ 2.5 โดยน้ำหนัก ผลจากการทดลองบ่งชี้ว่าทั้งความเป็นกรดและลักษณะเฉพาะของรูพรุนของตัวเร่งปฏิกิริยามีผลต่อการเปลี่ยนกรดโอเลอิกและการให้ผลผลิตมอนอโอเลอิน ซึ่งตัวเร่งปฏิกิริยา S-NN1-H40 แสดงประสิทธิภาพสูงที่สุดโดยให้ค่าการเปลี่ยนกรดโอเลอิก ร้อยละ 95 และให้ผลผลิตมอนอโอเลอิน ร้อยละ 56 นอกจากนั้นพบว่าการเติมหมู่ฟังก์ชันเอมีนบนวัสดุรองรับเอสบีเอ 15 ก่อนการเติมกรดทังสโตฟอสฟอริกช่วยเพิ่มการกระจายตัวของกรดทังสโตฟอสฟอริกบนวัสดุรองรับซึ่งส่งผลต่อประสิทธิภาพในการเร่งปฏิกิริยาที่เพิ่มขึ้น ตัวเร่งปฏิกิริยา S-NN1-H40 ซึ่งเป็นตัวเร่งปฏิกิริยาที่มีประสิทธิภาพที่สุดในงานวิจัยนี้สามารถนำกลับมาใช้ซ้ำได้อย่างน้อย 6 ครั้งโดยไม่สูญเสียประสิทธิภาพในการเร่งปฏิกิริยาอย่างมีนัยสำคัญ การศึกษาจลนศาสตร์ของปฏิกิริยาเอสเทอริฟิเคชันที่เร่งปฏิกิริยาด้วย S-NN1-H40 พบว่าเป็นปฏิกิริยาอันดับหนึ่งและมีค่าพลังงานก่อกัมมันต์เท่ากับ 35.45 กิโลจูลต่อโมล

ภาควิชา เคมี	ลายมือชื่อนิสิต .....
สาขาวิชา เคมี	ลายมือชื่อ อ.ที่ปรึกษาหลัก .....
ปีการศึกษา 2560	ลายมือชื่อ อ.ที่ปรึกษาร่วม .....

5771919523 : MAJOR CHEMISTRY
KEYWORDS: ESTERIFICATION / HETEROGENEOUS CATALYST / TUNGSTOPHOSPHORIC ACID / AMINE-FUNCTIONALIZED SBA-15 / MESOPOROUS SILICA

KULLATIDA RATCHADAPIBAN: SELECTIVE ESTERIFICATION OF GLYCEROL WITH OLEIC ACID USING TUNGSTOPHOSPHORIC ACID SUPPORTED ON FUNCTIONALIZED MESOPOROUS SILICA. ADVISOR: WIPARK ANUTRASAKDA, Ph.D., CO-ADVISOR: DUANGAMOL TUNGASMITA, Ph.D., 87 pp.

A series of protonated amine-functionalized SBA-15 materials was successfully prepared. Each sample of mesoporous SBA-15 was first functionalized with each of the three types of amino-organosilanes: APTES (N), AAPTMS (NN), and DETTMS (NNN). Each of the resulting materials was then protonated with Keggin-type tungstophosphoric acid (HPW) at two different concentrations: 20 wt.% (H20) and 40 wt.% (H40). The six types of materials obtained were labelled as S-N1-H20, S-N1-H40, S-NN1-H20, S-NN1-H40, S-NNN1-H20, and S-NNN1-H40. The materials were fully characterized by XRD, N_2 adsorption-desorption, FT-IR, SEM/EDX, TEM, and elemental analysis. The characterization results show that the synthesized materials exhibited highly ordered hexagonal mesoporous rope-like structure, indicating that the structure of the SBA-15 support was preserved after the modification with amino-organosilanes and HPW. The surface area, pore diameters, and acidity of the synthesized materials were in the range of 55 to 299 $m^2 g^{-1}$, 6.18 to 7.05 nm, and 0.18 to 0.49 mmole g^{-1}, respectively.

The synthesized materials were tested as catalysts for the esterification of glycerol with oleic acid to produce monoolein using a glycerol/oleic acid molar ratio of 4:1 at 160 °C for 3 h and with 2.5 wt.% of catalyst loading. The results indicate that the conversion of oleic acid and the yield of monoolein were influenced by the acidity and pore characteristics of the catalysts. In particular, S-NN1-H40 exhibited the highest oleic acid conversion (95%) and monoolein yield (56%). Functionalizing SBA-15 with aminosilanes prior to HPW addition was also found to enhance the distribution of HPW throughout the support and, in turn, improved the catalytic efficiency. The best-performing catalyst in this study, S-NN1-H40, also exhibited good reusability whereby no significant loss in catalytic activity was observed for at least six catalytic cycles. The kinetics of the esterification catalyzed by S-NN1-H40 was first order with an activation energy of 35.45 kJ mol^{-1}.

Department:	Chemistry	Student's Signature	.....
Field of Study:	Chemistry	Advisor's Signature	.....
Academic Year:	2017	Co-Advisor's Signature	.....

ACKNOWLEDGEMENTS

First of all I would like to express deepest gratitude to Dr. Wipark Anutrasakda, my advisor and Dr. Duangamol Tungasamita, my co-advisor for their excellent guidance and invaluable advice in this research. I am really thankful to them for their teaching and encouragement throughout the course of research. The thesis would not have been completed without all of the support from them.

I would like to gratefully thank to the chairperson, Assoc. Prof. Dr. Vudhichai Parasuk and thesis committee, Dr. Numpon Insin and Dr. Kittisak Choojun for all of their kindness and useful suggestions in the research.

I would like to special thanks to the members of Materials Chemistry and Catalysis Research Unit for their willing helps and friendships, especially Ms. Padtaraporn Chanhom, Mr. Chawalit Takoon, Ms. Wishulada Injumpa, Ms. Jamornpan Yangcharoenyuenyong, Mr. Apichat Klayanon, Ms. Apakorn Phasuk and Ms. Chutima Tangku.

Furthermore, I wish to mention and forward a complete gratitude to my family for all of their loves and support throughout my graduate study. Finally, I am really thankful to Mr. Chitchon Wangkran for his sincere kindness and encouragement.

CONTENTS

Page

Page

Page

Page

LIST OF TABLES

LIST OF FIGURES

LIST OF SCHEMES

LIST OF ABBREVIATIONS

S	=	Santa Babara Amorphous no.15 (SBA-15)
N	=	3-aminopropyltriethoxysilane (APTES)
NN	=	[3-(2-aminoethylamino)propyltrimethoxysilane] (AAPTMS)
NNN	=	(Trimethoxysilylpropyl)diethylenetriamine (DETTMS)
H20	=	20 weight percent of tungstophosphoric acid (HPW)
H40	=	40 percent by weight of tungstophosphoric acid (HPW)
int	=	Internal standard
wt.%	=	Percent by weight
mg	=	Milligram
g	=	Gram
mmole	=	Millimole
mL	=	Milliliter
L	=	Liter
M	=	Molar
˚C	=	Degree Celsius
K	=	Kelvin
mm	=	miliimeter

LIST OF ABBREVIATIONS (Continued)

μm	=	Micrometer
nm	=	Nanometer
m^2	=	Square meter
cm^3	=	Cubic centimeter
kJ	=	Kilo-joule

CHAPTER I

INTRODUCTION

1.1 Theory

1.1.1 Catalysts

A catalyst is a chemical substance that affects the chemical reaction rate. Generally, a catalyst provides an alternative route of reaction by lowering the activation energy (Ea) required for the reaction [1]. The activation energy of reaction with the presence of a catalyst is lower than that of the uncatalyzed reaction as shown in Fig. 1.1.

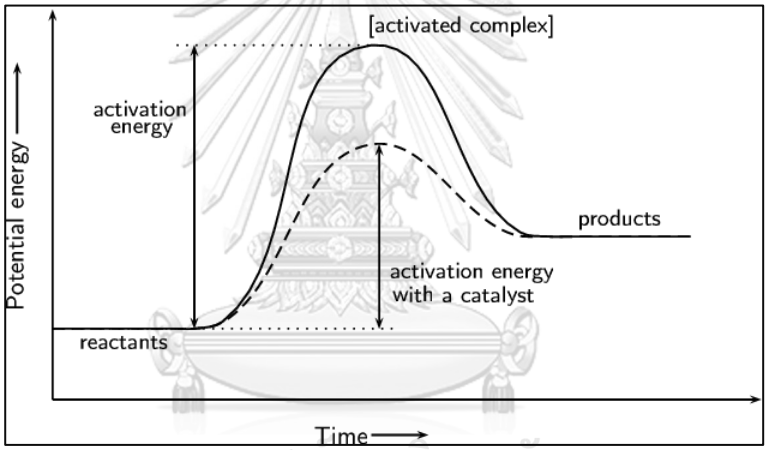

Figure 1.1 Potential energy diagram of general reaction and the effect of a presence of a catalyst on the reaction: solid line represents non-catalyzed reaction and dash line represents catalyzed reaction. [2]

Maxwell-Boltzmann distribution is a plot between the number of particles and kinetic energy. The Maxwell-Boltzmann distribution of a reaction with and without the presence of catalyst is shown in Fig. 1.2. Only particles that have energies equal to or higher than activation energy (Ea) can be reacted or collided with other particles to succeed in the reaction to form products. To make the particles that do not have energy higher than the activation energy react with others, the addition of a catalyst is a solution [3]. From the diagram, the addition of

a catalyst leads to a decrease in activation energy, causing the increasing number of particles that have high enough energies to complete the reaction [4].

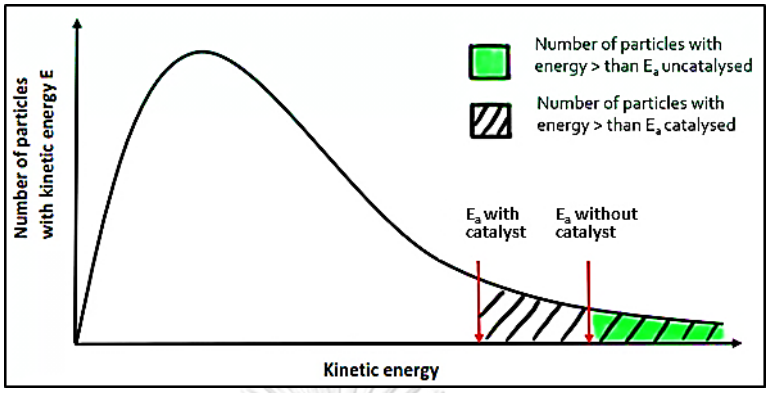

Figure 1.2 Maxwell-Boltzmann distribution. [5]

1.1.1.1 Type of catalysts

Catalysts can be generally classified into two types as homogeneous catalysts and heterogeneous catalysts.

1.1.1.1.1 Homogeneous catalysts

A homogeneous catalytic reaction is a reaction in which a catalyst and reactants are in the same physical phase [6]. Normally, most of homogeneously catalyzed reactions occur in a gas or liquid phase. In addition, homogeneous catalysts are highly selective but they are difficult to be separated from the reaction mixture.

1.1.1.1.2 Heterogeneous catalysts

A heterogeneous catalytic reaction is a reaction in which a catalyst and reactants form separate physical phases. The heterogeneous catalyst is usually in a solid form and the reactants are in a liquid or gas phase. Porous materials such as zeolites [7, 8] and mesoporous silicas [9, 10] are commonly used as supporting materials for heterogeneous catalysts. Heterogeneous catalytic reactions normally occur at the surface of the catalysts because the active sites of catalysts such as metal complexes, acids, and bases, usually are functionalized or immobilized on the surface of supporting materials [11-13]. Although the catalytic activity of heterogeneous catalysts are normally not as good as that of

homogeneous catalysts, heterogeneous catalysts are more stable at high temperature and easy to be separated from the reaction mixture [14, 15]. The comparison of properties of homogeneous and heterogeneous catalysts is shown in Table 1.1.

Table 1.1 Comparison of properties of homogeneous and heterogeneous catalysts. [16, 17]

Factor	Homogeneous catalyst	Heterogeneous catalyst
Active sites	All atom (no phase boundaries)	Only active surface atom
Selectivity	High	Low
Diffusion problem	Absent	Present (mass transfer controlled)
Temperature of reaction	< 200°C (due to low thermal stability)	> 200°C (due to high thermal stability)
Reusability	A lack of reusability	Easy to be reused by filtration/centrifugation
Application	Limited	Wide (complex structures for specific work can be designed.)

1.1.2 Porous materials

Porous materials are the focus of intensive research in recent years, due to their extremely promising properties for many applications especially in heterogeneous catalysis [9, 18-20]. Porous materials can be classified by their pore sizes, based on International Union of Pure Applied Chemistry (IUPAC), into three types as shown in Table 1.2 and Fig. 1.3.

Table 1.2 Classification of porous materials.

Type of porous material	Pore diameter
Micropore	< 2 nm
Mesopore	2 – 50 nm
Macropore	> 50 nm

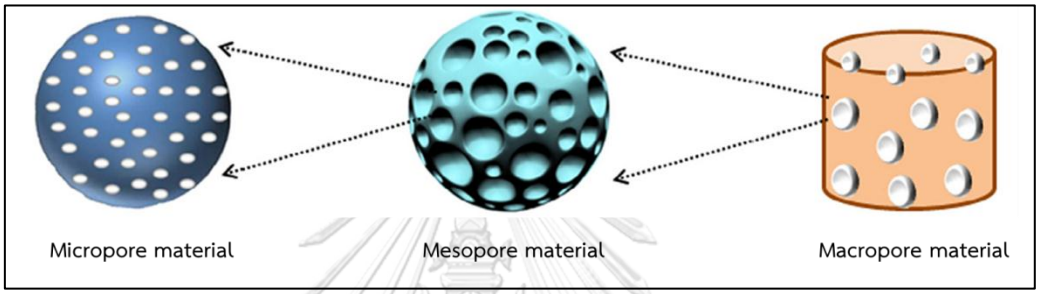

Figure 1.3 Types of porous materials. [21]

Zeolite materials are ones of interesting microporous materials in many fields but zeolites have a limitation in terms of the diffusion of some molecules into their small micropores. To overcome this limitation, mesoporous materials have been developed and employed in reactions involving the use of large starting materials.

1.1.3 Mesoporous materials

Mesoporous materials are materials with pore diameter in the range of 2 to 50 nanometers. Mesoporous materials have many shapes of pores, such as, hexagonal, cubic, and lamellra, depending on templates used in the synthesis. Examples of mesopore structures are shown in Fig. 1.4.

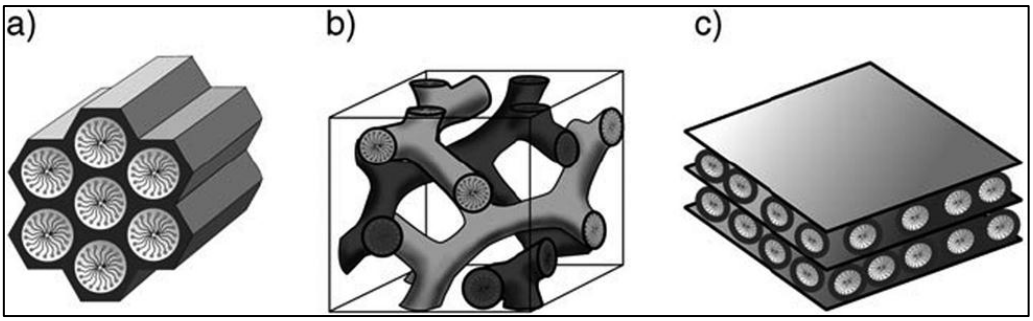

Figure 1.4 Examples of mesopore structures: a) hexagonal, b) cubic, and c) meso-lamellar. [22]

1.1.3.1 Classification of mesoporous materials

Mesoporous materials can be classified into three categories based on synthetic procedures as shown in Table 1.3.

Table 1.3 Classification of mesoporous materials by synthetic procedure. [23]

Assembly	Template	Media	Material
Electrostatic	quaternary ammonium salt	base or acid	MCM-41
H-bonding	primary amine	neutral	HMS
H-bonding	amphiphilic triblock copolymer	acid (pH<2)	SBA-15

1.1.3.2 Synthesis strategies of mesoporous materials

The formation of mesoporous materials depends on the interaction between organic species (silica source) and inorganic species (surfactant or template). Typically, the surfactants are amphiphilic molecules which are composed of two parts: hydrophilic head and hydrophobic tail on the alkyl chain side as shown in Fig. 1.5.

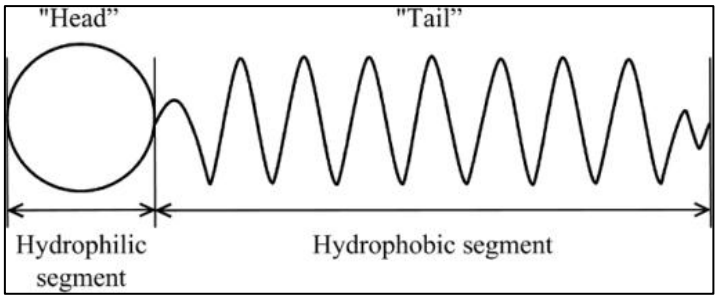

Figure 1.5 Component of surfactant. [24]

Different synthesis strategies are required for different surfactants to maintain the interaction with the inorganic parts. Surfactants are classified into three types depending on their charging properties [25]:

(I) Anionic surfactants (S^-), with negatively charged hydrophilic head (ex. phosphate, sulphonate, and alkyl carboxylate).

(II) Cationic surfactants (S^+), with positively charged hydrophilic head (ex. quarternary ammonium salt).

(III) Non-ionic surfactants (S^0), with electrostatic neutral hydrophilic head (ex. ethyloxide/propyloxide diblock or triblock copolymer).

Charge of surfactants (S) is considered as an intrinsic property while charge of silica precursors is dependent on the pH of synthesis system compared to the isoelectric point (p*I*) of silica which is ~1.2. Silica species is neutral at its isoelectric point, is negative at pH above p*I* and, is positive at pH below p*I* [26]. Table 1.4 shows the different interactions between the organic species and inorganic species in the formation of mesoporous materials. As shown in Fig. 1.6, interactions between the inorganic species and the head groups of organic species or surfactants with charge in Fig. 1.6 (a)-(d) are mainly electrostatic forces. In case of Figure 1.6 (e)-(f), the interactions between neutral inorganic and organic species are hydrogen bonding.

Table 1.4 Different types of interaction between inorganic species and surfactants in the formation of mesoporous materials. [23]

Surfactant type	Inorganic type	Interaction type	Example materials
Cationic (S^+)	I^-	S^+I^-	MCM-41, MCM-48
	I^+X^-	$S^+X^-I^+$	SBA-1, SBA-2, zinc phosphate
	I^0F^-	$S^+F^-I^0$	silica
Anionic (S^-)	I^+	S^-I^+	Al, Mg, Mn, Ga
	I^-M^+	$S^-M^+I^-$	alumina, zinc oxide
Neutral S^0 or N^0	I^0	S^0I^0	HMS, MSU-X, aluminum oxide
	I^+X^-	$S^0X^-I^+$	SBA-15

Where: S^x represents surfactant with charge of x

I^x represents silica species with charge of x

X^- represents inorganic salt (usually a halide)

M^+ represents mediator cation (ex. Na^+ and K^+)

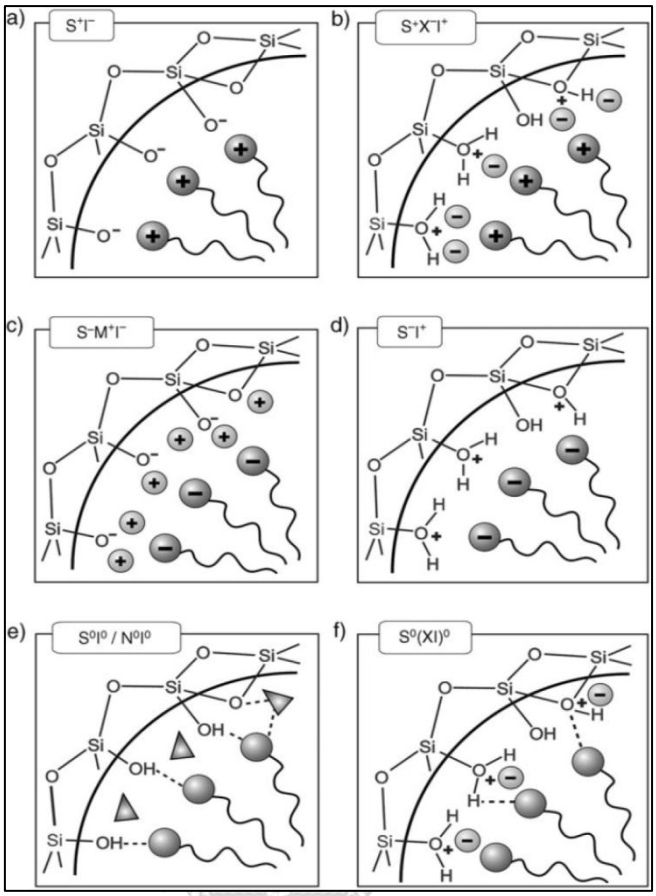

Figure 1.6 Schematic of the different types of interaction between silica and surfactant. [26] (Dash line represents hydrogen bond)

1.1.3.3 Mechanistic formation of mesoporous materials

The liquid crystalline templating mechanism is shown in Scheme. 1.1. There are two pathways to form mesoporous materials. Pathway *a*, surfactant liquid crystals, a template for mesopores, are introduced to form micelles before silica source is added. The inorganic species are deposited at the hydrophilic part of the template which has the same geometry of liquid crystalline phase. Then, the template is removed to form mesoporous silica materials. In the other pathway called cooperative self-assembly (pathway *b*), the template or surfactant of mesopores is formed after the addition of silica source. The silica source controls the self-assembly process of the template to form mesoporous materials.

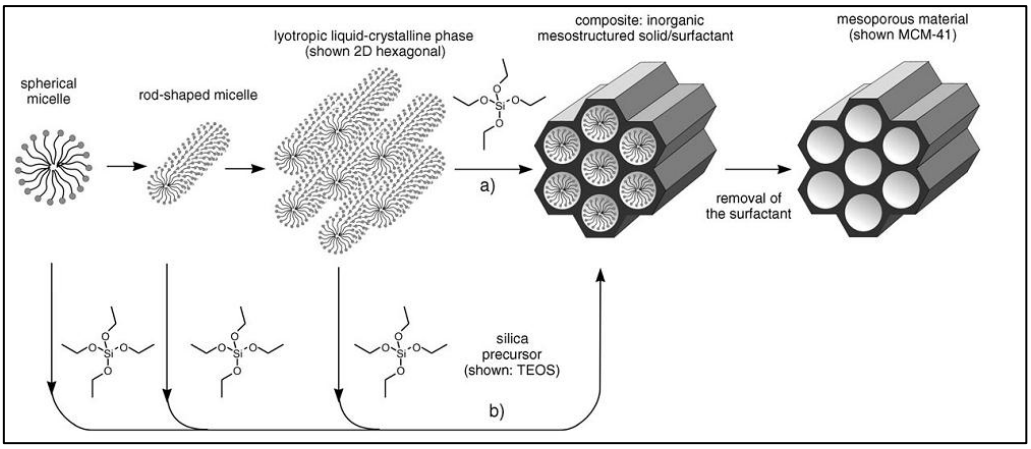

Scheme 1.1 Mechanism of mesoporous silica formation by liquid crystalline templating and cooperative self-assembly mechanisms. [22]

1.1.4 Santa Barbara Amorphous No.15 material (SBA-15)

Hexagonal array of pores namely as Santa Barbara Amorphous no. 15 was developed in 1998 by Zhao et al. [27] as shown in Fig. 1.7. The SBA-15 mesoporous silica material was produced under acidic condition using amphiphilic triblock copolymers template consisting of a central PPO hydrophobic block with two PEO hydrophilic blocks linked at its two extremities and tetraethyl orthosilicate (TEOS) as a silica source. The unique properties of SBA-15 such as high surface area (>700 m^2 g^{-1}), narrow pore size distribution (2-10 nm), large pore volume (>0.9 cm^3 g^{-1}), high thermal and chemical stabilities, and non-toxic material [28] make it well suitable for various applications such as a supporting material for catalysis [29], drug delivery [30], environmental analysis for adsorption and separation [31], and biosensor [32]. Moreover, one of the most important advantages of SBA-type materials is the thickness of their walls (3.1 to 6.4 nm), which is significantly thicker than those of other mesoporous materials such as MCM-type silicas (1 to 1.5 nm) [33, 34]. In addition, SBA-type materials have larger pore diameters than MCM-type materials [35] as shown in Fig. 1.8.

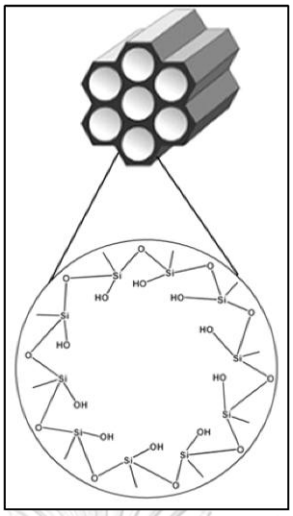

Figure 1.7 Hexagonal structure of Santa Babara Amorphous no.15 (SBA-15). [36]

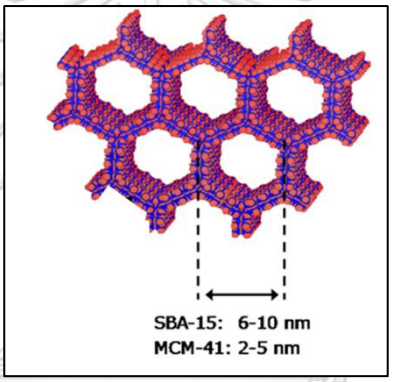

Figure 1.8 Different pore diameters of SBA-type and MCM-type materials. [37]

1.1.4.1 Formation of SBA-15 material

Blin and Clerc [38] reported the formation mechanism of SBA-15 material as shown in Fig. 1.9. The formation of SBA-15 is composed of six steps:

(a) Initial dissolution of P123 to form spherical micelles.

(b) Addition of the silica precursor (TEOS in this case).

(c) Hydrolysis of the silica species, the beginning of the condensation of silica precursors, and some oligomers of silica beginning to interact with ethylene oxide (EO) groups at the surface of the surfactant micelles.

(d) Shape transformation of spherical-shaped hybrid organic–inorganic micelles to rod-like shape.

(e) Nucleation of the hexagonal mesophase.

(f) The hexagonal phase of mesoporous silica SBA-15 obtained.

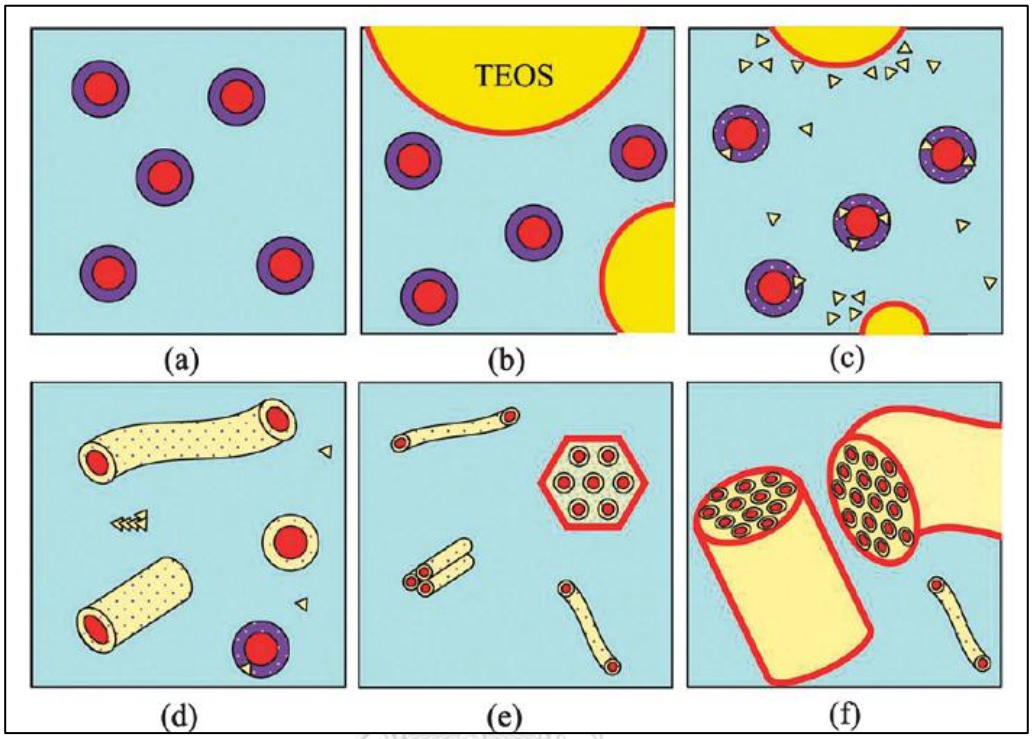

Figure 1.9 Formation mechanism of SBA-15 material. [38]

1.1.4.2 Modification of SBA-15 material

Mesoporous silica SBA-15 has a well-defined structure and contains high density of silanol groups on the surface. A wide range of organic functional groups such as amine, alcohols, thiols, sulfonic acid, and carboxylic acid [39, 40] can be used to functionalize on to the surface of SBA-15. The different functional groups on the surface of SBA-15 can play several roles in various applications. For example, in the medicine studies, functionalized SBA-15 can enhance drug adsorption capacity or slow-down rate of drug release to target cell [41]. In catalysis works, functionalized organic molecules on SBA-15 as heterogeneous catalysts can enhance the catalytic activity by increasing the acidic or basic active sites of the catalysts and size of organic molecules can control the selectivity of products in terms of shape selectivity property.

1.1.4.3 Shape selectivity

Shape selective catalytic reactions are reactions that depend on the pore structure of the catalyst and the size of reactant and product molecules. Shape selectivity of porous materials can be divided into three types (Fig. 1.10) [42]:

(I) Reagent selectivity: This shape selectivity restricts the accessibility of reactants into the pore of the catalyst.

(II) Transition state selectivity: This shape selectivity is about preventing the formation of intermediate compounds whose sizes are larger than the pore size of the catalyst.

(III) Product selectivity: This shape selectivity prevents bulky products from diffusing out of the pore. Instead, they are converted into less bulky products to be able to diffuse out of the catalyst channels.

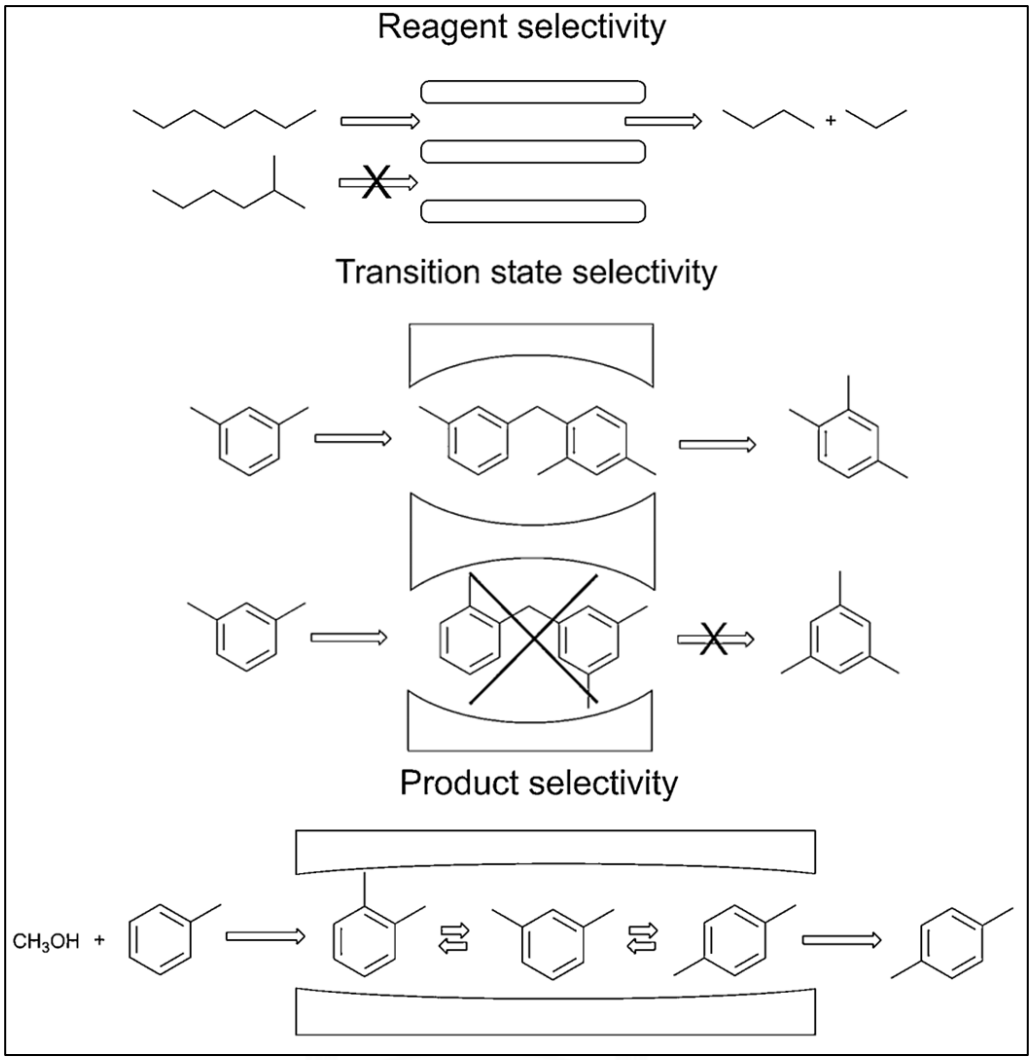

Figure 1.10 Three types of shape selectivity in porous channels. [43]

1.1.5 Tungstophosphoric acid (HPW)

Heteropoly acids are compounds in which one atom of the following elements: B, Al, Si, P, As, etc. is combined with a number of atom of an element, such as, V, Nb, Mo, Ta, or W, along with a relatively large number of oxygen atoms [44, 45]. Heteropoly acids, especially tungstophosphoric acid ($H_3PW_{12}O_{40}$, or HPW) with a kegging structure, have received much attention in the past decade among acid catalysts for a wide range of reactions [46-48].

The Keggin structure was first discovered by J.F Keggin [44] in 1934. Keggin ions have a general formula of $[X^{n+}M_{12}O_{40}]^{(8-n)-}$, where X is a heteroatom of B^{3+}, Si^{4+}, or P^{5+}, M is the metal atom (usually Mo and W), and O represents oxygen

atom [49]. The anions possess tetrahedral symmetry and are composed of a cage of twelve tungsten atoms linked by oxygen atoms with the phosphorus atom at the center as shown in Fig. 1.11 [50].

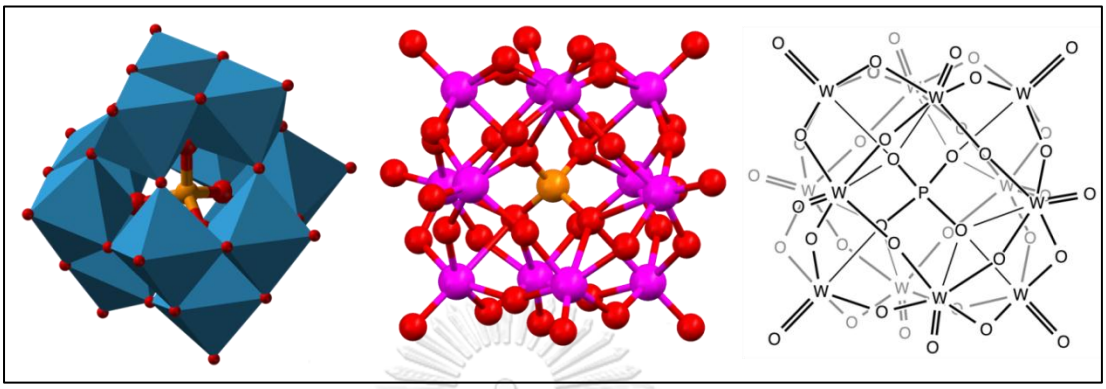

Figure 1.11 Keggin structure of tungstophosphoric acid. [51]

Tungstophosphoric acid (HPW) has been used in many applications, such as, sensor [52], adsorption [53], and catalysis [54], due to its outstanding high acid strength. HPW is a stronger Brønsted acid than most mineral acids and it has low corrosivity, making it an attractive catalyst in a variety of reactions [55-57]. However, bulk HPW has a disadvantage of low surface area (< 10 $m^2 g^{-1}$), which leads to an inefficient accessibility of reactant molecules to the strong acid sites [58]. To overcome this problem, much recent researches have been focused on the use of HPW incorporated on porous materials such as mesoporous silica [59], zeolite [60], and polymer [61], resulting in the improvement of surface area and activity of the catalysts. Given that HPW has a diameter of ~1.2 nm, it can be incorporated inside the pores of mesoporous materials in order to improve its surface area and thermal stability [62]. Although, HPW supported porous materials show high catalytic activity, the incorporated HPW on the surface of supporting materials can be easily leached out, especially in polar media due to the weak interaction of HPW and supporting materials [63]. Xie and Hu [64] suggested a strategy to overcome this problem by functionalizing organic compounds on supporting materials prior to HPW addition in order to form a strong interaction of HPW with organic molecules *via* ionic bond, resulting in high dispersion of HPW with minimal leaching and improving the reusability of the catalyst.

1.1.6 Esterification

Esterification is a chemical reaction for the production of esters from carboxylic acids and alcohols as shown in Scheme 1.2. Basically, the reaction rates of esterification reactions are slow when the reactions are performed without the presence of catalyst [65]. Commonly, acid catalysts are used to speed up the rates of esterification reactions. The acid catalyzed esterification mechanism is shown in Scheme 1.3.

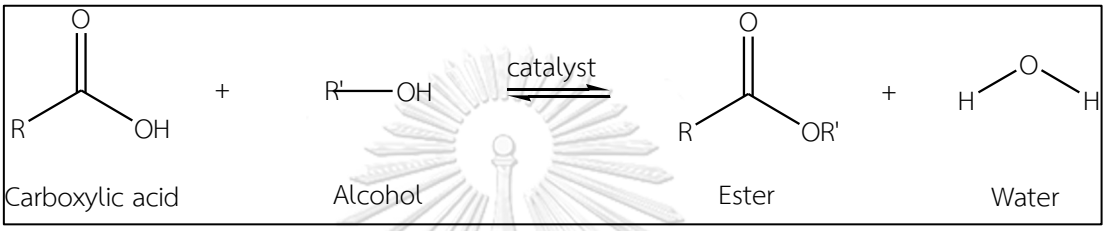

Scheme 1.2 General esterification reaction.

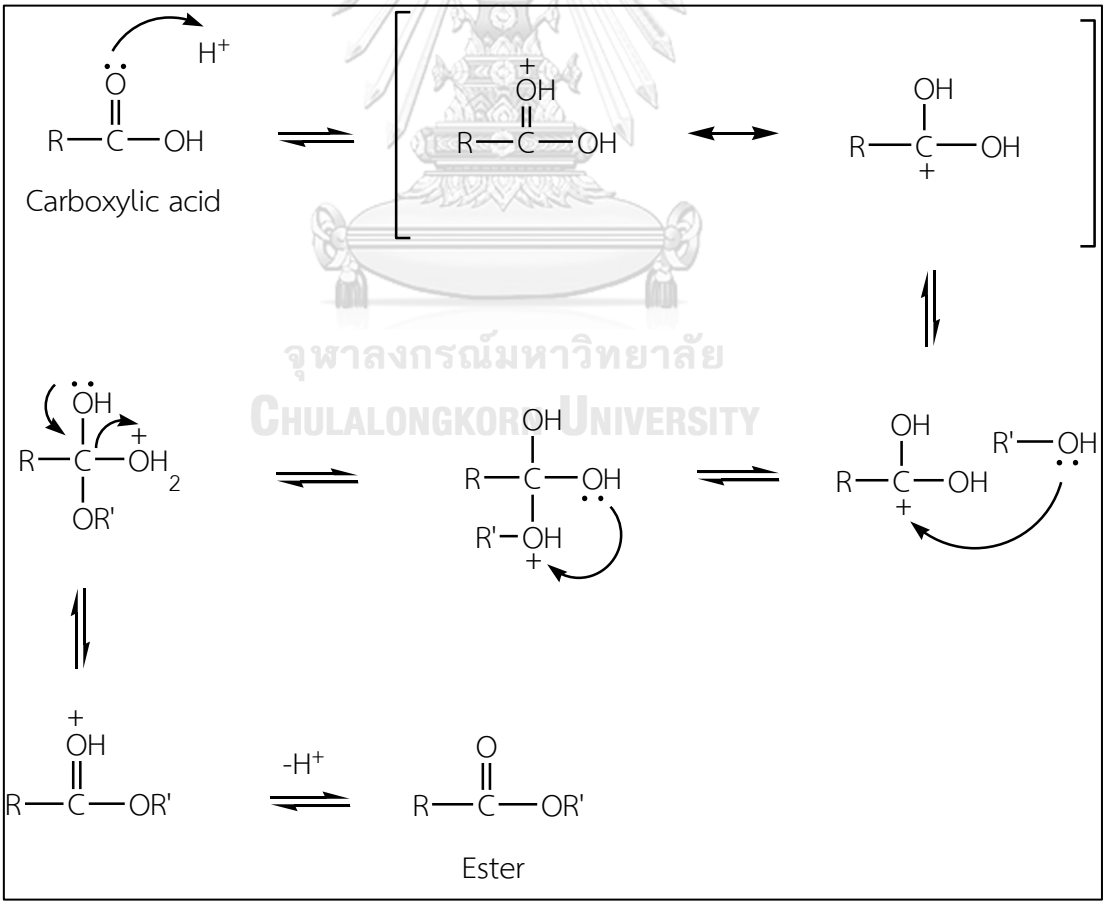

Scheme 1.3 Mechanism of esterification reaction. [23]

The mechanism of esterification consists of six steps [66]:

(i) A proton transfer from the acid catalyst to an oxygen of the carboxylic acid increases electrophilicity of the carboxylic carbon.

(ii) The positive charge is delocalized between the oxygen and carbon atoms.

(iii) The positively-charged carbon is attacked by the nucleophilic oxygen atom of the alcohol.

(iv) A proton transfer from the bottom oxygen atom to one of the others occurs.

(v) A water molecule is removed from the ion.

(vi) Deprotonation occurs to produce the ester product.

1.1.6.1 Esterification of glycerol with free fatty acids (FFAs)

1.1.6.1.1 Reaction pathways

Several researchers studied reaction pathways of esterification of glycerol with free fatty acids to produce glyceride products [67-69]. Based on their investigation, the reaction pathways of glycerol with free fatty acids esterification are classified into two types:

(i) Consecutive reaction pathway (Scheme 1.4): A mono glyceride is formed from the reaction of glycerol and a fatty acid. The diglyceride and triglyceride are then formed from the reaction of the fatty acid with the produced monoglyceride and with the produced diglyceride, respectively.

(ii) Irreversible parallel reaction pathway (Scheme 1.5): All of mono-, di-, and triglyceride products are directly produced from the reaction of glycerol and free fatty acids, and not from the reaction between monoglyceride and free fatty acids or diglyceride and free fatty acids.

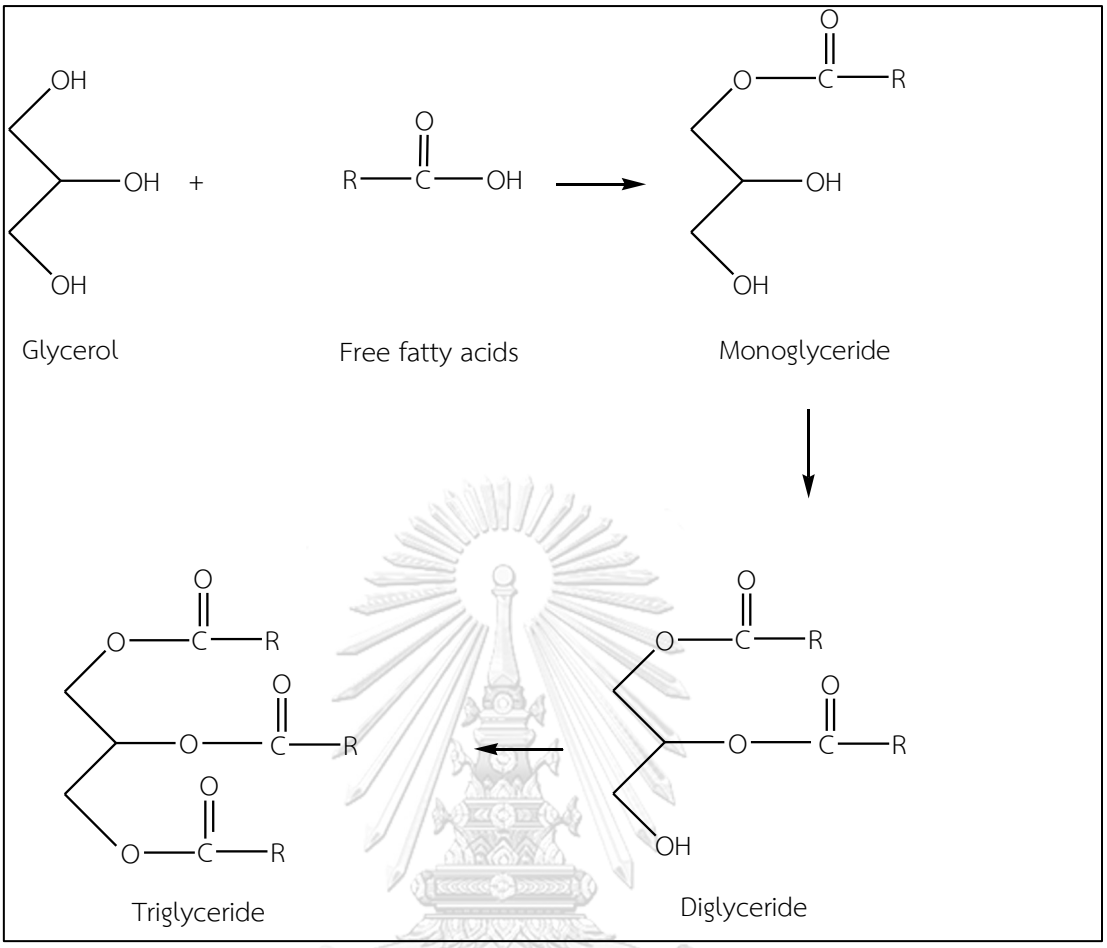

Scheme 1.4 Consecutive reaction pathway for the esterification of glycerol with free fatty acids. [67]

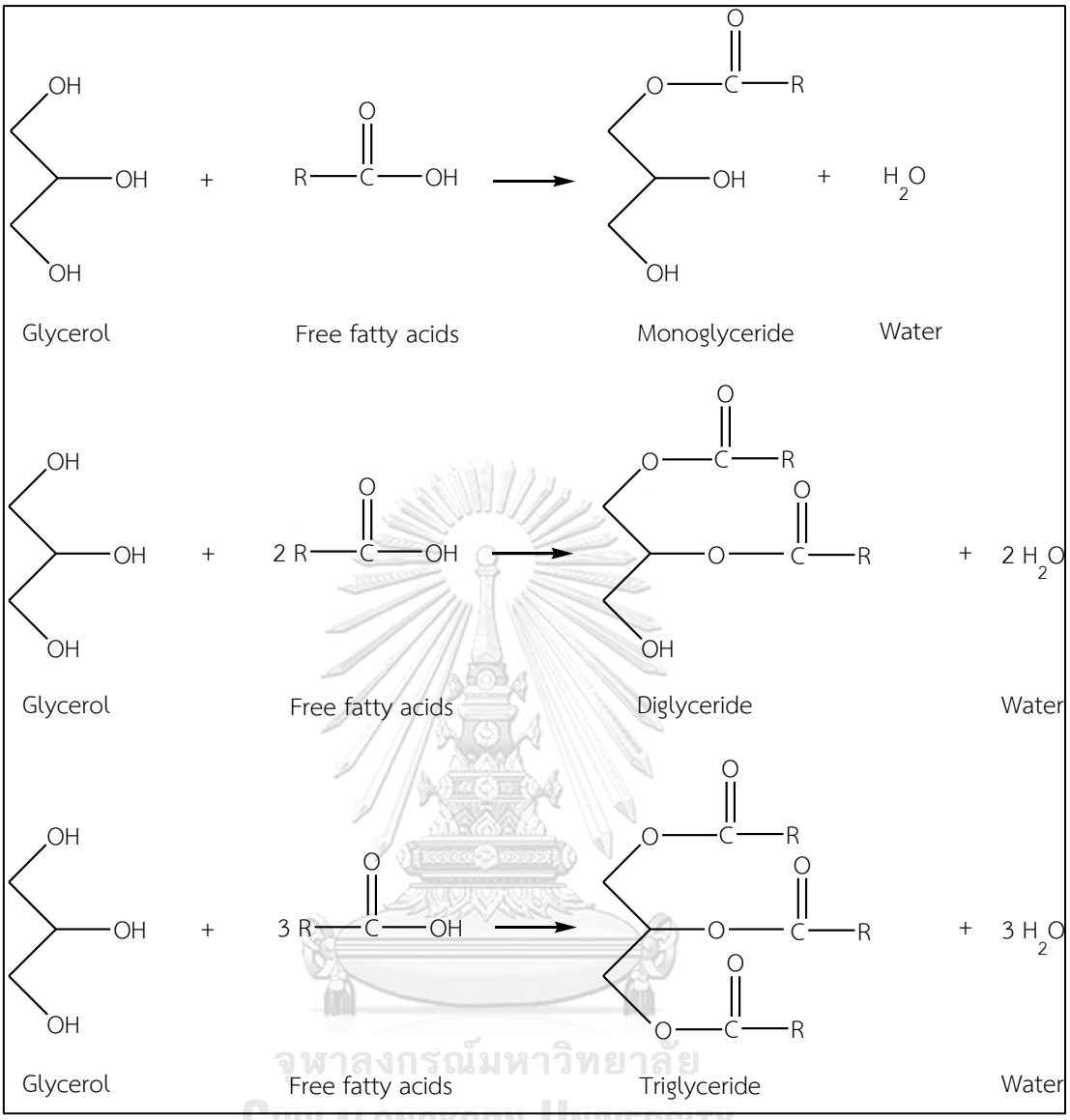

Scheme 1.5 Irreversible parallel reaction pathway for the esterification of glycerol with free fatty acids. [68]

1.2 Literature reviews

1.2.1 Catalysts for esterification and related reactions

Conventionally, homogeneous catalysts, such as, sulfuric acid, phosphoric acid, and heteropolyacids, are used in esterification reactions. Homogeneous catalysts generally exhibit high catalytic activity because they are in the same phase as reactants and therefore the reactants can easily travel to and react at active sites of the catalysts [54, 70]. In addition, the preparation of homogeneous catalysts is normally not complicated.

De Godói Silva et al., [54] studied catalytic activity of homogeneous Brønsted acids: tungstophosphoric acid (HPW), p-toluene sulfonic acid (PTSA), and sulfuric acid (H_2SO_4) on esterification of ethanol and oleic acid. The results showed that the use of HPW, PTSA, and H_2SO_4 catalysts led to the conversion of 92%, 8%, and 19%, respectively. This finding was explained that $PW_{12}O_{40}^{3-}$ species was a softer base than SO_4^{2-} species, leading to the shift of the equilibrium towards a higher concentration of H^+ species. Therefore, the reaction with HPW catalyst had a higher H^+ concentration and then gave a higher conversion and a higher yield of the ester product.

Moquin and Temelli [70] used supercritical carbon dioxide as a catalyst for esterification of glycerol and oleic acid. The reaction was carried out in a batch stirred reactor using glycerol to oleic acid molar ratios of 10:1, 1:1, and 1:2 at 10 MPa, and 250 °C. The results showed that the decrease in glycerol to oleic acid molar ratio would promote the formation of diolein and triolein rather than monoolein probably due to lack of accessible glycerol and the presence of an excess amount of oleic acid.

Although, the use of homogeneous catalysts for esterification reactions is effective in terms of high conversion and high product yield, they are difficult to be recovered and reused in the new catalytic cycles. In addition, the esterification reactions with homogeneous catalysts require high temperature at 220-250 °C [70, 71]. Consequently, the use of high temperature results in undesired changes in color

and taste of desired ester products as well as low selectivity of desired ester products.

Therefore, much of recent research has shifted to the use of heterogeneous catalysts to overcome the problems mentioned by using suitable supporting materials, such as, activated carbon [72], titania [73], silica [74], zeolites [75], and mesoporous silica [76] materials. Mesoporous silicas are widely used as catalyst supports because they possess some unique advantages including high surface area and pore volume, narrow pore size distribution, good thermal and chemical stability, and facile surface functionalization. In terms of surface functionalization, mesoporous silicas can be functionalized with acid, base, or organic molecules, such as, heteropolyacid, sulfuric acid, and amino organosilane molecules.

Tropecêlo et al., [77] used various heteropolyacids, such as, tungstophosphoric acid (HPW), molybdophosphoric acid (HPMo), and tungstosilicic acid (HSiW) impregnated on SBA-15 material and used them as heterogeneous catalysts for esterification of palmitic acid with methanol. The results showed that the conversions of palmitic acid using HPW, HPMo, and HSiW incorporated SBA-15 catalysts were 92%, 57%, and 45%, respectively. The SBA15-HPW catalyst gave better activity than SBA15-HPMo and SBA15-HSiW mainly because HPW exhibited higher acid strength than that of the other two heteropolyacids.

Patel and Singh [55] studied esterification of glycerol with acetic acid using tungstophosphoric acid (HPW) anchored to MCM-41. The reaction was carried out at 100 ºC for 3 h with the glycerol to acetic acid molar ratio of 1:6. They synthesized the catalysts by the impregnation method using 10-40% of HPW anchored to MCM-41 supporting material. The results showed that the glycerol conversion was increased with the increase in the loading amount of HPW in the catalyst. Specifically, the 30% HPW/MCM-41 catalyst gave the highest conversion of glycerol at 87%. However, the glycerol conversion was decreased when 40% HPW/MCM-41 was used as the catalyst because the active sites on the catalyst might be blocked. For the reaction with 30% HPW/MCM-41 catalyst, the ester product

distribution was 25% of monoacetylglycerol, 60% of diacetylglycerol, and 15% of triacetylglycerol.

Calleja et al., [78] synthesized amine functionalized SBA-15 material as an adsorbent of CO_2 at low pressure. They synthesized SBA-15 by a hydrothermal method using Pluronic P123 as a structure directing agent and tetraethyl orthosilicate (TEOS) was used as a silica source. Then, SBA-15 was functionalized with three different organosilanes: aminopropyl (N), ethylene-diamine (NN), and diethylene-triamine (NNN) silanes. The results showed that the CO_2 adsorption capacities on N-, NN-, and NNN-functionalized materials were 48.8, 60.0, and 76.8, respectively. The results indicate that the amounts of adsorbed CO_2 increased with the increase in the nitrogen amounts present in the materials, related to a chemisorption mechanism.

Xie and Hu [64] reported the acidolysis of soybean oil with caprylic and capric acids using SBA-15-pr-NH_2-HPW catalyst. They added different amounts of HPW (30%, 50%, and 70 wt.%) into the catalysts to study their activity. The measured acid concentrations were 0.31, 1.02, and 1.12 mmol g^{-1} for 30% SBA-15-pr-NH_2-HPW, 50% SBA-15-pr-NH_2-HPW, and 70% SBA-15-pr-NH_2-HPW, respectively. The results showed that the highest conversions of caprylic (62.2%) and of capric acid (64.5%) were obtained from the reaction with the 70% SBA-15-pr-NH_2-HPW catalyst mainly due to its highest acidity.

1.2.2 Esterification of glycerol with free fatty acids

Glycerides can be produced by esterification reactions of glycerol with carboxylic acids in basic or acidic condition. In general, most of researchers studied esterification of glycerol with short-chain and medium-chain carboxylic acids ($C<12$) such as acetic acid [59, 79], benzoic acid [80], cinnamic acid [81], and capric acid [82]. The number of reports on esterification of glycerol with long-chain carboxylic acids ($C \geq 12$) is significantly less than that with short-chain and medium-chain carboxylic acids probably because the esterification reactions with short-chain and medium-chain acids tend to give higher conversions and higher rates of reaction, as compared to the esterification reactions with long-chain acids. These observations can be partly

attributed to differences in the solubility of carboxylic acids with different chain lengths in reaction mixtures. In the literature reviews, some researchers studied the effect of chain length of carboxylic acids on the conversion of reactants and on the selectivity of the ester products, as described below. [83, 84]

Kotwal and Srinivas [83] studied the effect of chain length of four fatty acids: lauric acid (C_{12}), myristic acid (C_{14}), stearic acid ($C_{18:0}$), and oleic acid ($C_{18:1}$) on esterification reaction with glycerol using Fe–Zn double-metal cyanide catalyst. The results showed that the conversions of lauric acid, myristic acid, stearic acid, and oleic acid were 75.0%, 75.9%, 62.2%, and 63.4%, respectively. It is clearly seen that the conversion of fatty acids decreased with an increase in the fatty acid chain length. The explanation could be because glycerol is better-miscible with shorter-chain fatty acids than with longer-chain fatty acids, leading to higher activity and higher conversion. In addition, the longer-chain fatty acids might partially block the active sites of the catalyst, resulting in the difficulty of glycerol to approach the active sites of the catalyst and generate the products.

Freitas et al. [84] reported monoglyceride selectivity from the esterification of glycerol with different chain-length fatty acids: lauric acid (C_{12}), myristic acid (C_{14}), palmitic acid (C_{16}), stearic acid ($C_{18:0}$), and oleic acid ($C_{18:1}$) using ***Penicillium camembertii*** lipase immobilized on epoxy SiO_2-PVA composite as the catalyst. The selectivity of monoglyceride was 59.45%, 47.92%, 45.86%, 42.16%, and 32.92% for lauric acid, myristic acid, plamitic acid, stearic acid, and oleic acid, respectively. The shortest-chain fatty acid (lauric acid) exhibited the highest selectivity of monoglyceride, as compared to the other fatty acid reactants. This might be explained that the long-chain free fatty acids had much lower reaction rates for the formation of monoglycerides.

The esterification reactions of glycerol with medium-chain and long-chain free fatty acids such as lauric acid, palmitic acid, and oleic acid using a wide range of catalysts were also reported in other works.

An et al. [85] synthesized a series of arenesulfonic acid-functionalized alkyl-bridged organosilica hollow nanospheres, Si(R)Si-ArSO_3H-HNS, with different bridging alkyl groups (R groups): ethyl, phenyl, or biphenyl in the silica and tested their activity in the esterification of glycerol and lauric acid. The results showed that monolaurate yields were 35.4%, 30.8%, and 30.1% for Si(Ph-Ph)Si-ArSO_3H-HNS, Si(Ph)Si-ArSO_3H-HNS, and Si(Et)Si-ArSO_3H-HNS catalysts, respectively. The Si(Ph-Ph)Si-ArSO_3H-HNS gave the highest catalytic activity in esterification due to its high Brønsted acidity and its smallest pore diameter compared to the other catalysts.

Hamerski and Corazaa [86] used a layered double hydroxide of Mg–Al–CO_3 as a catalyst for esterification of glycerol with lauric acid. They investigated the effect of reaction temperature ranging from 100 - 180 °C and fixed the glycerol and lauric acid molar ratio at 3:1 with 2% catalyst loading. At high temperature (180 °C), the glycerol conversion reached 99% while it was merely 25% at low temperature (100°C). The glycerol conversion was favored at high temperature because the reaction was an endothermic reaction.

Yusoff and Abdullah [10] synthesized monopalmitin from the esterification reaction of glycerol with palmitic acid using sulfated zirconia supported on SBA-15 as a catalyst. They studied two factors affecting palmitic acid conversion and yield of glyceride products. The first factor was the effect of reaction temperature (160-180 °C). The conversion of palmitic acid increased with increasing temperature. This observation agreed with Hamerski and Corazaa's work as described above [86]. The palmitic acid conversion at 160 °C, 170 °C, and 180 °C were found to be 76%, 86% and 96%, respectively. The second factor was the effect of catalyst loading (1-3 wt.%). The results showed that conversion of palmitic acid and monopalmitin yield were increased with the increase of catalyst loading, likely due to the increasing number of acidic sites on the catalyst.

Singh et al. [87] synthesized monoolein and diolein from the esterification of glycerol with oleic acid using zirconia supported on zeolite as a catalyst. They studied the effect of oleic acid to glycerol molar ratios of 1:2, 1:4, and 1:6 with 0.5 wt.% of catalyst loading at 150 °C. The results showed that the oleic

acid conversion increased when the molar ratios of oleic acid to glycerol increased from 1:2 to 1:4. However, when the molar ratio was increased to 1:6, the conversion of glycerol was not further increased. This finding could be caused by an excess amount of glycerol, which might hinder the formation and diffusion of molecules in the mesopores of the catalyst.

According to the literature reviews described above, in the present study, we decided to use tungstophosphoric acid (HPW), which is a type of heteropolyacids, as the acid catalyst in the esterification of glycerol and a long-chain fatty acid, oleic acid. Tungstophosphoric acid was chosen mainly because it is a stronger acid than other mineral Brønsted acids. Moreover, tungstophosphoric acid, which possesses a Kegging-type, is more attractive than other types of heteropolyacids due to its high acid strength, high thermal stability, and low corrosion resistance. Nevertheless, Kegging-type heteropolyacids have a few disadvantages: low surface area, high solubility in water. Therefore, they cannot be employed by themselves, as heterogeneous catalysts. One way to solve this problem is to immobilize Kegging-type heteropolyacids on suitable supporting materials such as mesoporous silica SBA-15.

In this work, we first prepared amino-functionalized SBA-15 materials. Three aminosilanes with different number of amino groups were used to functionalize on SBA-15. Then, the obtained amino-functionalized SBA-15 materials were protonated at the amino sites using tungstophosphoric acid. Finally, the as-prepared materials were tested as the catalysts in the esterification of glycerol with oleic acid ($C_{18:1}$).

1.3 Objectives

1.3.1 To prepare a series of protonated amine-functionalized SBA-15 materials using three types of aminosilanes as the amine source and tungstophosphoric acid as the acid source.

1.3.2 To characterize the synthesized materials using XRD, surface area analysis, FT-IR, SEM/EDX, TEM, and elemental analysis.

1.3.3 To investigate the catalytic activities of the synthesize materials as heterogeneous catalysts for the esterification reaction of glycerol with oleic acid to produce monoolein.

1.4 Scope

This research focused on the synthesis and characterization of a series of protonated amine-functionalized SBA-15 materials using mesoporous SBA-15, three types of amino-organosilanes: APTES (N), AAPTMS (NN), and DETTMS (NNN), and tungstophosphoric acid as the starting materials. The synthesized materials were then used as heterogeneous catalysts to test and compare their catalytic activities for the esterification reaction of glycerol with oleic acid to produce monoolein. In addition, catalyst reusability and kinetic studies were also explored.

CHAPTER II

EXPERIMENTS

2.1 Apparatus and analytical techniques

2.1.1 Powder X-ray diffraction (XRD)

All of the XRD patterns were recorded on Rigaku, Dmax 2200/utima+ X-ray powder diffractometer with a monochromator and Cu Kα radiation operated at 40 kV and 30 mA. The diffraction patterns of pure SBA-15 and modified SBA-15 materials were recorded in the 2-theta range of 0.7 to 5.0 degree with a scan speed of 2 degrees/min and a scan step of 0.02 degree. The scattering, the divergent, and the receiving slits were fixed at 0.05 degree, 0.5 degree, and 0.15 mm, respectively. The synthesized materials containing tungtophosphoric acid were also recorded in the 2-theta range of 10.0 to 80.0 degree with a scan speed of 5 degrees/min and a scan step of 0.02 degree. The scattering, the divergent, and the receiving slits were fixed at 0.5 degree, 0.5 degree, and 0.3 mm, respectively.

2.1.2 Surface area analysis

The textural properties of the materials were examined by nitrogen adsorption–desorption method using a BELSORP, mini-II nitrogen adsorptometer. The samples were degassed for 2 h at 400 °C and 110 °C for pure SBA-15 and modified SBA-15, respectively. Specific surface areas were calculated using Brunauer–Emmett–Teller (BET) equation. The Barrett-Joyner-Halanda (BJH) model was used to determine total pore volumes and pore sizes.

2.1.3 Elemental analysis (EA)

Elemental analysis was used to determine the weight percentage of nitrogen present in amine functionalized SBA-15 materials using Thermo flash 2000 organic elemental analyzer.

2.1.4 Fourier transform infrared spectroscopy (FT-IR)

The FT-IR technique was used to verify functional groups present in the synthesized materials. All of FT-IR spectra were recorded by the impact 410 (Nicolet) using the transmission mode in the range of 4000-400 cm^{-1}.

2.1.5 Scanning electron microscopy (SEM)

The morphology and particle sizes of pure SBA-15 and modified SBA-15 materials were acquired on JSM-6480LV (JEOL) scanning electron microscope combined with Energy Dispersive X-ray spectroscope (EDX) oxford instrument. The samples were dispersed in ethanol and dropped on carbon sticky tape mounted on sample holders and coated the samples with gold.

2.1.6 Transmission electron microscopy (TEM)

The mesoporous channels and particles sizes of prepared mesoporous materials were performed on JEM-2100 (JOEL) transmission electron microscope. The samples were dispersed in ethanol and dropped on copper grids.

2.1.7 Gas chromatography analysis (GC)

Conversion of oleic acid and selectivity of monoolein, diolein, and triolein were analyzed by a Varian CP-3800 gas chromatograph equipped with a flame ionization detector (FID) and a 10 m length x 0.53 mm metal column with a split ratio of 1:50. The maximum temperature of the metal column was 400 °C. For the measurement, one microliter of a sample was injected into a metal column with the temperature program described in Table 2.1.

Table 2.1 The GC temperature program for analysis

Temperature (°C)	Rate (°C/min)	Hold (min)
50	-	1
180	15.0	0
230	7.0	0
370	10.0	5

2.2 Chemicals and reagents

Table 2.2 List of chemicals

Chemicals	Suppliers
Tetraethyl orthosilicate (TEOS)	Aldrich
Triblock copolymer pluronic (P123)	Aldrich
3-aminopropyltriethoxysilane (APTES)	Aldrich
[3-(2-aminoethylamino)propyl]trimethoxysilane] (AAPTMS)	Alfa Aesar
3-(trimethoxysilylpropyl)diethylenetriamine (DETTMS)	Aldrich
Phosphotungstic acid hydrate (HPW)	Sigma-Aldrich
Glycerol ($C_3H_8O_3$)	Sigma-Aldrich
Oleic acid ($C_{18}H_{34}O_2$)	Fluka
Eicosane ($C_{20}H_{42}$)	Aldrich
Sodium hydroxide (NaOH)	Merck
Sodium chloride (NaCl)	Carlo Erba reagents
Potassium hydrogen phthalate (KHP)	Merck
Molecular sieve 4A	Sigma-Aldrich
Acetone (C_3H_6O)	RCI Labscan
Ethanol (C_2H_5OH)	RCI Labscan
Toluene ($C_6H_5CH_3$)	RCI Labscan
Tetrahydrofuran (THF)	RCI Labscan

2.3 Preparation of catalysts

2.3.1 Synthesis of SBA-15 material

The SBA-15 mesoporous material with an ordered structure was hydrothermally prepared according to a published procedure [27], which involved the use of the triblock co-polymer Pluronic P123 as a surfactant template in acidic conditions. Briefly, 20.0 g of P123 was dissolved in a 600 mL solution of 2.0 M HCl and the mixture was stirred at room temperature. After a clear solution obtained, 42.5 g of tetraethyl orthosilicate (TEOS) was added dropwise into the above solution

at room temperature under vigorously stirring. The solution was stirred for 1 h and then aged under stirring at 40 ℃ for 24 h. The resulting white gel was transferred into teflon-lined autoclaves for the hydrothermal process at 100 ℃ for 48 h. The product was recovered by filtration, washed with deionized water several times, and dried at 100 ℃ overnight. Finally, the as-prepared material was calcined at 550 ℃ for 5 h to remove the template using the temperature program shown in Fig. 2.1.

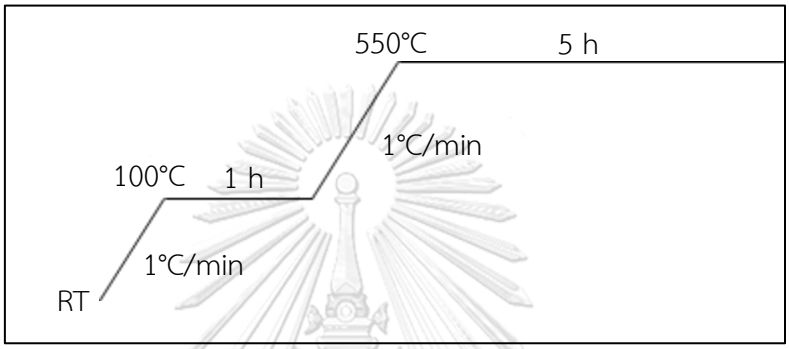

Figure 2.1 A temperature program used for the template removal from SBA-15.

2.3.2 Synthesis of amine-functionalized SBA-15 materials

The amine functionalized SBA-15 materials were prepared by a post-grafting synthesis method using three organosilane molecules containing different numbers of amino groups (Fig. 2.2):

(i) 3-aminopropyltriethoxysilane (APTES), which contains one primary amino group and is denoted as N

(ii) [3-(2-aminoethylamino)propyltrimethoxysilane] (AAPTMS), which contains one primary and one secondary amino groups and is denoted as NN

(iii) 3-(trimethoxysilylpropyl)diethylenetriamine (DETTMS), with one primary and two secondary amino groups and is denoted as NNN.

The procedure was modified from a published literature [31]. Typically, 1 g of the calcined SBA-15 was refluxed in 50 mL of anhydrous toluene. Then, a required amount of an amino-organosilane was added to the mixture dropwise. The reaction was refluxed at 110 ℃ for 24 h under nitrogen atmosphere. The resulting solid was separated from the mixture by centrifugation, washed with ethanol, and dried at 60

°C overnight. An example for the preparation of amine functionalized SBA-15 materials was illustrated in Scheme 2.1 and the designated names of each material are presented in Table 2.3.

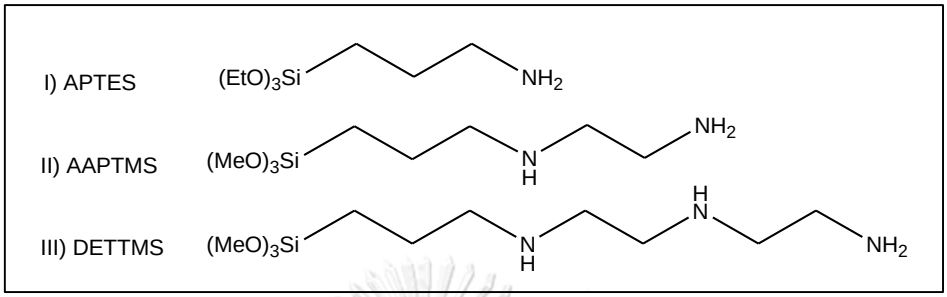

Figure 2.2 Chemical structures of amino-organosilanes.

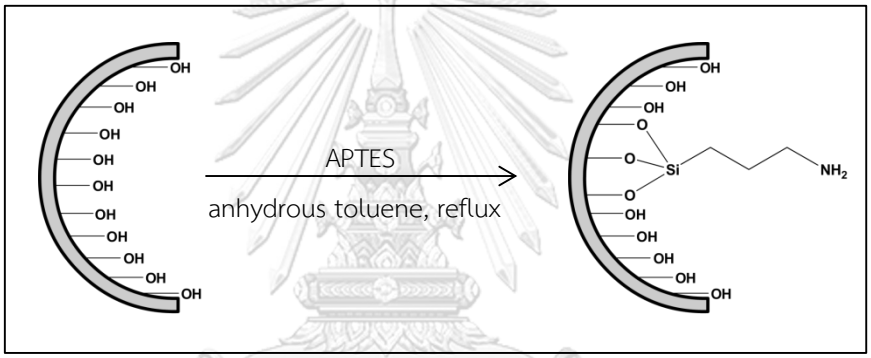

Scheme 2.1 Post-grafting synthesis of APTES-functionalized SBA-15.

Table 2.3 Designated names of amine-functionalized SBA-15 materials.

Materials	SBA-15	Ligands	Amount of ligand added (wt.%)
S-N1	1 g	APTES	49
S-N3			74
S-N5			83
S-NN1		AAPTMS	49
S-NN3			74
S-NN5			83
S-NNN1		DETTMS	49
S-NNN3			74
S-NNN5			83

2.3.3 Acidification of the prepared materials with tungstophosphoric acid (HPW)

Tungstophosphoric acid was incorporated into amine-functionalized SBA-15 materials by an impregnation method reported by Zhang and coworkers [88]. Briefly, 0.5 g of each amine-functionalized SBA-15 material was added into 60 mL of deionized water. Then, a required amount (20 and 40 weight percent) of HPW was added into the solution under a continuous stirring at room temperature for 24 h. Finally, the obtained product was washed with deionized water and acetone for several times and dried at room temperature. An example for the preparation of acidified amine functionalized SBA-15 materials was shown in Scheme 2.2. According

to the results from elemental analysis, the percentages of nitrogen were similar across all the materials synthesized using the same type of aminosilane at different initial amounts (ranging from 1-5 mL). In other words, using higher amount of aminosilane did not lead to more grafting of aminosilane on the surface of SBA-15, probably due to the steric effect caused by amine chains distributed on the surface of SBA-15. Therefore, only 1 mL of each type of amino-organosilane was used to graft the amino groups on the surface of SBA-15 prior to the impregnation of HPW. For comparison, tungstophosphoric acid was also incorporated into pure SBA-15 with the same procedure described above. The designated names of each acidified materials are presented in Table 2.4.

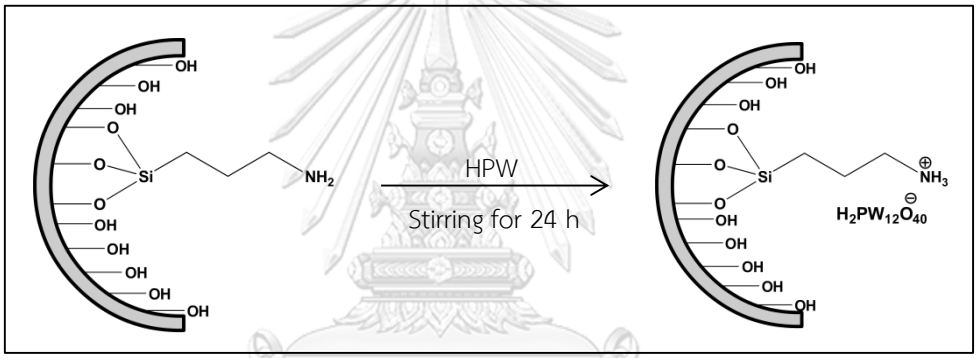

Scheme 2.2 Impregnation method for HPW anchored APTES-functionalized SBA-15 synthesis.

Table 2.4 Designated names of acidified mesoporous materials.

Materials	Amine-functionalized SBA-15	HPW added (% wt.)
S-N1-H20	0.5 g of S-N1	20
S-NN1-H20	0.5 g of S-NN1	
S-NNN1-H20	0.5 g of S-NNN1	
S-H20	0.5 g of SBA-15	
S-N1-H40	0.5 g of S-N1	40
S-NN1-H40	0.5 g of S-NN1	
S-NNN1-H40	0.5 g of S-NNN1	
S-H40	0.5 g of SBA-15	

2.3.4 Acid-base titration

2.3.4.1 Standardization of NaOH with KHP

0.02XX g of KHP was dissolved in deionized water and the volume of the solution was adjusted to 100.00 mL using a volumetric flask. Then, 20.00 mL of the prepared KHP solution was titrated with 0.001X M NaOH using phenolphthalein as an indicator.

2.3.4.2 Titration of the prepared acidic catalysts with NaOH

The acid capacities of the prepared catalysts were examined according to a previous report [89] with some modifications. Briefly, 0.04 g of each catalyst was added into 12 ml of 2.0 M NaCl solution (ion-exchange agent) under stirring for 3 h at room temperature and titrated with 0.001X M NaOH using phenolphthalein as an indicator.

2.4 Catalytic esterification of glycerol with oleic acid

The procedure for esterification of glycerol with oleic acid was adapted from a previously published article [10]. The reaction was carried out in a two-necked round bottom flask equipped with an oil bath, a water-cooled condenser, and a magnetic stirring bar under nitrogen atmosphere. In general, the reaction was performed with a 4:1 molar ratio of glycerol and oleic acid and 2.5 weight percent of a catalyst at 160 °C for 10-300 min. After the reaction was stopped, the used catalyst was separated from the reaction mixture by high speed centrifugation. Remained oleic acid and ester products were derivatized with N-methyl-N-trimethylsilyltrifluoroacetamide and analyzed by GC-FID with a metal column. Eicosane was used as the internal standard for the GC measurements. Oleic acid conversion, product selectivity, and product yields were calculated as follows:

$$\text{Conversion (\%)} = \frac{\text{Initial mole of oleic acid - Final mole of oleic acid}}{\text{Initial mole of oleic acid}} \times 100$$

$$\text{Yield of monoolein (\%)} = \frac{\text{Mole of monoolein produced}}{\text{Initial mole of oleic acid}} \times 100$$

$$\text{Selectivity of monoolein (\%)} = \frac{\text{Mole of monoolein produced}}{\text{(Mole of monoolein produced) + 2(Mole of diolein produced) + 3(Mole of triolein produced)}} \times 100$$

2.5 Factors affecting yields of glyceride products

2.5.1 Effect of reaction time

The reaction time was varied in the range of 10-300 min with the glycerol/oleic acid molar ratio of 4:1 at 160 °C and 2.5 weight percent of catalyst loading.

2.5.2 Effect of reaction temperature

The reaction was performed as the general procedure above with the glycerol/oleic acid molar ratio of 4:1 for 3 h and 2.5 weight percent of catalyst loading at the reaction temperature range of 120-160 °C.

2.5.3 Effect of catalyst loading

The effect of catalyst loading was also studied. The amount of catalyst was varied from 0 to 3.5 weight percent using glycerol/oleic acid molar ratio of 4:1 at 160 °C for 3 h.

2.5.4 Effect of reactants ratio

The molar ratio of glycerol and oleic acid were investigated with the general condition described above. The effect of glycerol/oleic acid molar ratio was studied in the range of 1:1 to 6:1 at 160 °C for 3 h and 2.5 weight percent of catalyst loading.

2.6 Catalyst leaching test

The leaching test of HPW anions from the prepared acidic catalysts were investigated using a modified method described in a literature [90]. Briefly, 0.1 g of a catalyst was dispersed in 10 g of methanol. Then, the mixture was refluxed for 2 h. After that, the resulting mixture was centrifuged to separate the supernatant from the solid. The separated supernatant was measured by UV spectroscopy at the wavelength of 267 nm corresponding to the absorption band of $PW_{12}O_{40}^{3-}$ [90].

2.7 Reusability of catalysts

The method for catalyst reusability was adopted from a published work [91]. After the reaction was stopped, the used catalyst was separated from the reaction mixture by centrifugation and washed with cyclohexane and acetone and dried at 100 °C for 24 h before it was reused in the next cycle.

CHAPTER III
RESULTS AND DISCUSSIONS

3.1 Characterization of synthesized materials

3.1.1 Powder X-ray diffraction (XRD)

3.1.1.1 Powder X-ray diffraction of pure SBA-15 and amine-functionalized SBA-15 materials

Mesoporous silica SBA-15 was synthesized by a hydrothermal method according to a published procedure reported by Zhao et al. [27]. The XRD pattern of SBA-15 material, as shown in Fig. 3.1, exhibited three diffraction peaks at 2θ = 0.9°, 1.5°, and 1.8°, corresponding to (100), (110), and (200) reflection planes, respectively. The XRD result suggests 2D hexagonal mesoporous structure of SBA-15 with a space group of P6mm [92]. The pure SBA-15 was then functionalized with three types of amino-organosilanes: APTES (N), AAPTMS (NN), and DETTMS (NNN), using a post-grafting method modified from a published literature [31]. The XRD patterns of amine functionalized SBA-15 materials are shown in Fig. 3.1. The XRD patterns of all amine functionalized SBA-15 materials (S-N1, S-NN1, S-NNN1) still indicated a well-ordered 2D hexagonal (P6mm) pore arrangement which is a characteristic of SBA-15. This result suggested that the modified materials preserved the hexagonal structure of mesoporous SBA-15 [92]. However, the peak intensities of functionalized SBA-15 materials were decreased as compared to those of pure SBA-15 probably because amino-organosilane molecules incorporated on the surface of SBA-15 affected the crystallinity of the mesostructure but did not lead to a collapse of the SBA-15 channels [93]. In addition, the XRD peaks of functionalized SBA-15 materials were also slightly shifted to higher angles, indicating a decrease of the spacings between the crystallographic plane in SBA-15 [94]. Among the XRD peaks of the functionalized samples, the XRD peak due to the (100) plane of the S-NNN sample was found to be shifted to the highest angle, implying that DETTMS, the

most bulky amino-organosilane studied in this work, was successfully incorporated on the surface in the internal pores of SBA-15.

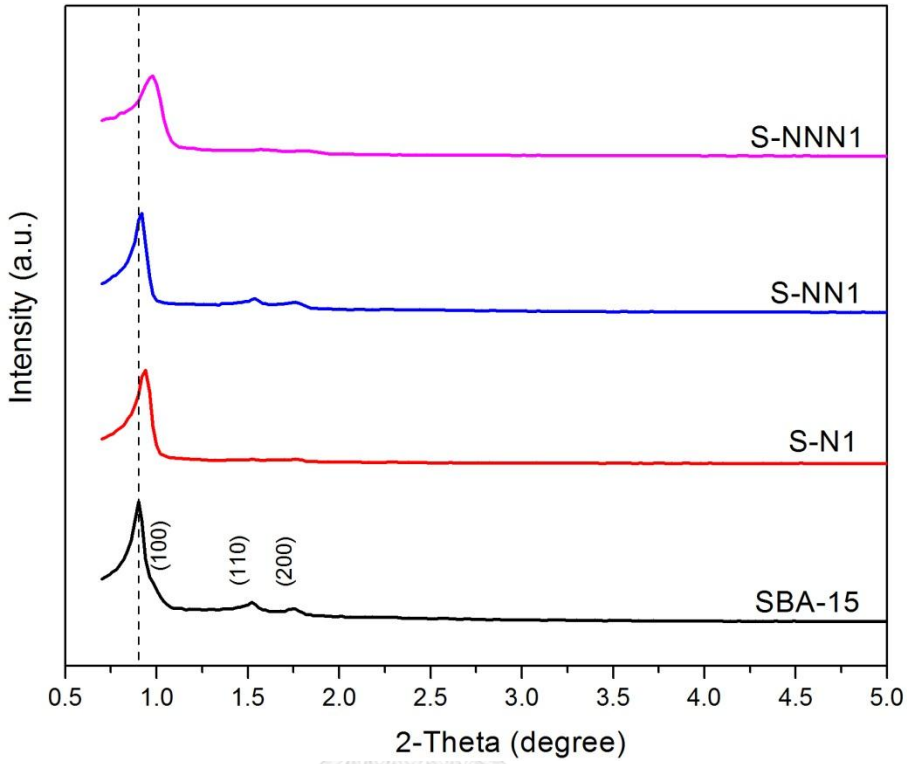

Figure 3.1 XRD patterns of SBA-15 and amine functionalized SBA-15 materials.

3.1.1.2 Powder X-ray diffraction of acidified amine-functionalized mesoporous silica SBA-15

The three amino-functionalized SBA-15 materials were acidified with 20 wt.% and 40 wt.% of tungstophosphoric acid (HPW) and their XRD patterns are shown in Fig. 3.2. The XRD patterns of all acidified samples exhibited the hexagonal structure similar to their parent SBA-15 material with a decrease in peak intensities, probably due to amino-organosilanes and HPW filled into the mesopores of SBA-15. In addition, the XRD peaks of all catalysts slightly shifted to higher 2θ values due to a decrease in *d*-spacings [95]. The XRD results indicated that the impregnation of HPW into amine-functionalized SBA-15 materials did not destroy the mesoporous structure of the support.

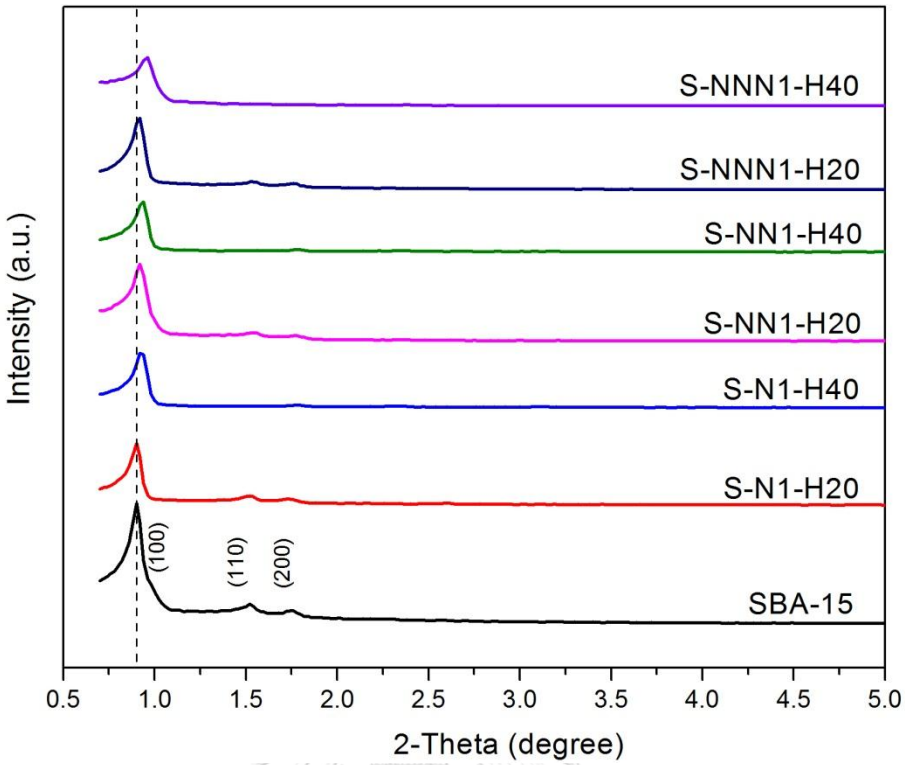

Figure 3.2 XRD patterns of pure SBA-15 and acidified amine-functionalized SBA-15.

3.1.2 N_2 adsorption-desorption

Pore characteristics of the synthesized materials were examined by N_2 adsorption-desorption technique. Surface areas of the synthesized materials were calculated from the Brunauer-Emmett-Teller (BET) method while their pore diameters and pore volumes were calculated from the Barret-Joyner-Halender (BJH) equation. Furthermore, internal and external surface areas were calculated from the *t*-plot equation. The textural properties of pure SBA-15 and acidified amine-functionalized SBA-15 materials are listed in Table 3.1. The pure SBA-15 material had a surface area of 729 $m^2 g^{-1}$ with a high internal surface area of 617 $m^2 g^{-1}$, a mean pore diameter of 8.06 nm, and a pore volume of 1.01 $cm^3 g^{-1}$. When SBA-15 was functionalized with amino-organosilanes and acidified with HPW, the surface areas of all modified materials were decreased. Specifically, the surface areas of the modified SBA-15 materials decreased with increasing the size of amino-organosilane molecules. For examples, the BET surface areas of S-N-H40, S-NN-H40, and S-NNN-H40 were 205, 177, and 55 $m^2 g^{-1}$, respectively.

According to the calculation from the *t*-plot equation, the internal surface area of the synthesized materials were significantly decreased after the surface modification with amino-organosilanes and HPW, implying that most of the amine groups and HPW were deposited in the mesopores of the support rather than on the external surface of the support. Mean pore diameter of the synthesized materials was decreased from 8.06 nm of the pure SBA-15 to 7.05 nm of the modified materials, except for the NNN-containing materials in which the pore size diameter was decreased to 6.18 nm. Pore volumes of S-N1/NN1-H20 and S-N1/NN1-H40 were decreased to ~0.6 and ~0.3 $cm^3 g^{-1}$, respectively; while, those of S-NNN1-H20 and S-NNN1-H40 were decreased to 0.2 and 0.06 $cm^3 g^{-1}$, respectively, probably due to the strong adsorption of protonated amine groups and HPW anions occurred mostly inside the channels of the modified supports [63]. Based on the results from N_2 adsorption-desorption and given that the sizes of glycerol and oleic acid, the starting materials for esterification reaction in this study, are 0.29 x 0.37 nm^2 and 1.27 x 1.76 nm^2, respectively, the starting materials are expected to diffuse efficiently to react at the acid sites of catalysts in the mesoporous channels.

Table 3.1 Textural properties of pure SBA-15 and acidified amino-functionalized SBA-15 materials.

Material	BET surface area ($m^2 g^{-1}$)	External surface area ($m^2 g^{-1}$)	Internal surface area ($m^2 g^{-1}$)	Pore diameter (nm)	Pore volume ($cm^3 g^{-1}$)
SBA-15	726	52	617	8.06	1.01
S-N1-H20	299	36	164	7.05	0.59
S-N1-H40	205	19	151	7.05	0.31
S-NN1-H20	295	38	159	7.05	0.57
S-NN1-H40	177	20	116	7.05	0.31
S-NNN1-H20	87	23	44	6.18	0.20
S-NNN1-H40	55	10	28	6.18	0.06

N_2 sorption isotherms of pure SBA-15 and acidified amine-functionalized SBA-15 materials are shown in Fig. 3.3. All of the isotherms of the prepared materials were categorized as type IV isotherms, a typical characteristic of mesoporous materials, according to the International Union of Pure and Applied Chemistry (IUPAC) classification [96]. In other words, after the modification of SBA-15, the structures of mesoporous silica were preserved, indicating that the functionalization with aminosilanes followed by the incorporation with HPW did not destroy the structure of the mesoporous structure of SBA-15.

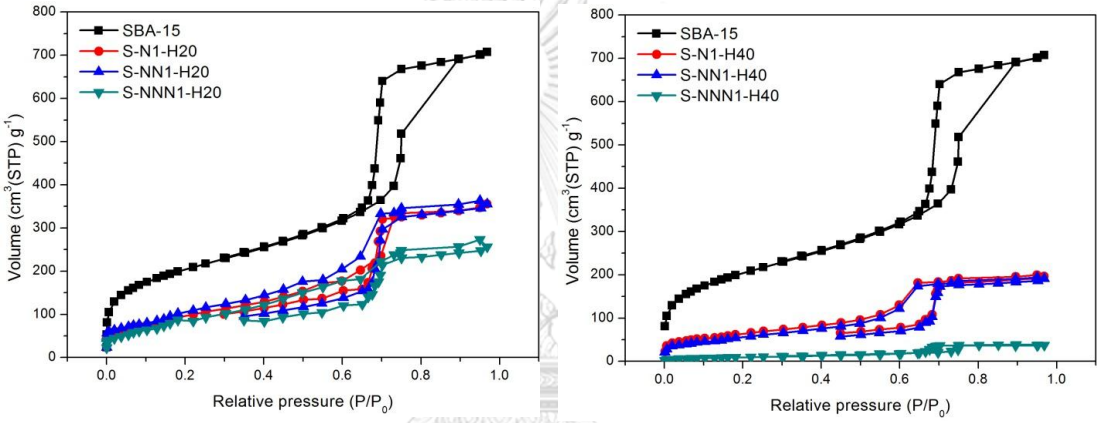

Figure 3.3 N_2 sorption isotherms of pure SBA-15 and acidified amine-functionalized SBA-15.

The pore size distribution of pure SBA-15 and acidified amine-functionalized SBA-15 are shown in Fig. 3.4. The results showed that the pore sizes of SBA-15 and all modified materials fell in the range of mesoporous sizes (2-21 nm). The shifts to smaller size distribution for all modified SBA-15 materials suggested the presence of protonated amines and incorporated HPW anions in the mesoporous channels of SBA-15. In addition, it was found that the synthesized materials with 20 wt.% HPW loading had larger pore sizes than those with 40 wt.% HPW loading probably because those with 40 wt.% of HPW contained more HPW anions in the pores and some HPW anions could also block the pore of the materials. Considering the effect of amino-organosilanes on pore size distributions, the pore size distributions of materials containing APTES (N) were quite similar to those containing AAPTMS (NN). However, the materials containing DETTMS (NNN)

showed significantly smaller pore sizes mesoporous. This could be resulted from two factors: 1) DETTMS is the most bulky aminosilane studied in this work 2) DETTMS possesses three amine groups that could be protonated by HPW while APTES and AAPTMS possess only one and two amine groups, respectively.

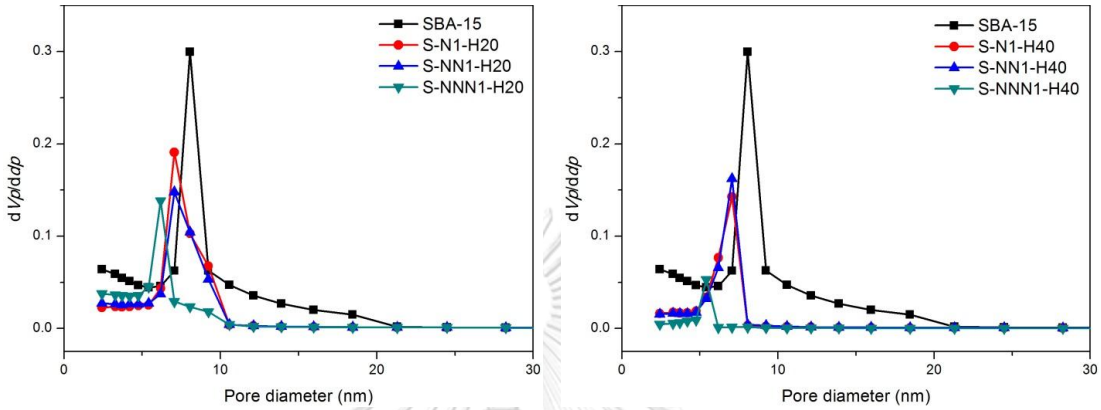

Figure 3.4 Pore size distributions of SBA-15 and acidified amine-functionalized SBA-15materials.

3.1.3 Fourier transform infrared spectroscopy

Fourier transform infrared spectroscopy (FT-IR) was used to confirm the presence of functional groups in the synthesized acidified amino-functionalized SBA-15 materials (Fig. 3.5). The spectra of all modified SBA-15 materials exhibited the following bands: O-H stretching (broad) at 3440 cm^{-1}; Si-OH bending vibration at 962 cm^{-1}; Si-O-Si asymmetric and symmetric stretching at 1084 and 800 cm^{-1}, respectively; and bending vibration of Si-O-Si at 467 cm^{-1}. This observation confirmed that the mesoporous structure of SBA-15 for all samples was retained after the surface modification with aminosilanes and HPW. The IR band due to water was observed at 1632 cm^{-1} in all modified SBA-15 samples. The presence of both water band (1632 cm^{-1}) and Si-OH band (3440 cm^{-1}) suggests the existence of hydrogen bonding formed between water molecules and hydrophilic Si-OH groups [29].

The peak due to P-O asymmetric stretching of pure HPW solid was observed at 1082 cm^{-1}. Furthermore, the characteristic peaks of pure HPW were found at 984, 893, and 810 cm^{-1}, which could be designated to the stretching

vibrations of terminal asymmetric oxygen ($W=O_d$), corner shared asymmetric oxygen ($W-O_b-W$), and edge shared oxygen ($W-O_c-W$), respectively [29]. For the modified SBA-15 materials, due to the interaction between the electron-rich $[PW_{12}O_{40}]^{3-}$ anions and the protonated amino-functionalized SBA-15 material, the red shifts of $W=O_d$ and $W-O_b-W$ stretching vibrations were observed. For example, the stretching vibrations of $W=O_d$, $W-O_b-W$ of the S-N1-H40 sample shifted to 943 and 881 cm^{-1}, respectively. The presence of these IR bands suggested the successful anchoring HPW on the amino-functionalized SBA-15 materials. Moreover, compared to IR spectra of pure SBA-15 and HPW, new peaks of the modified SBA-15 materials were observed in the region of 1468-1506 cm^{-1}, which might be ascribed to the signal of $-NH_3^+$ and $-NH_2^+-$ bending vibration, suggesting the successful protonation of the amino groups with HPW.

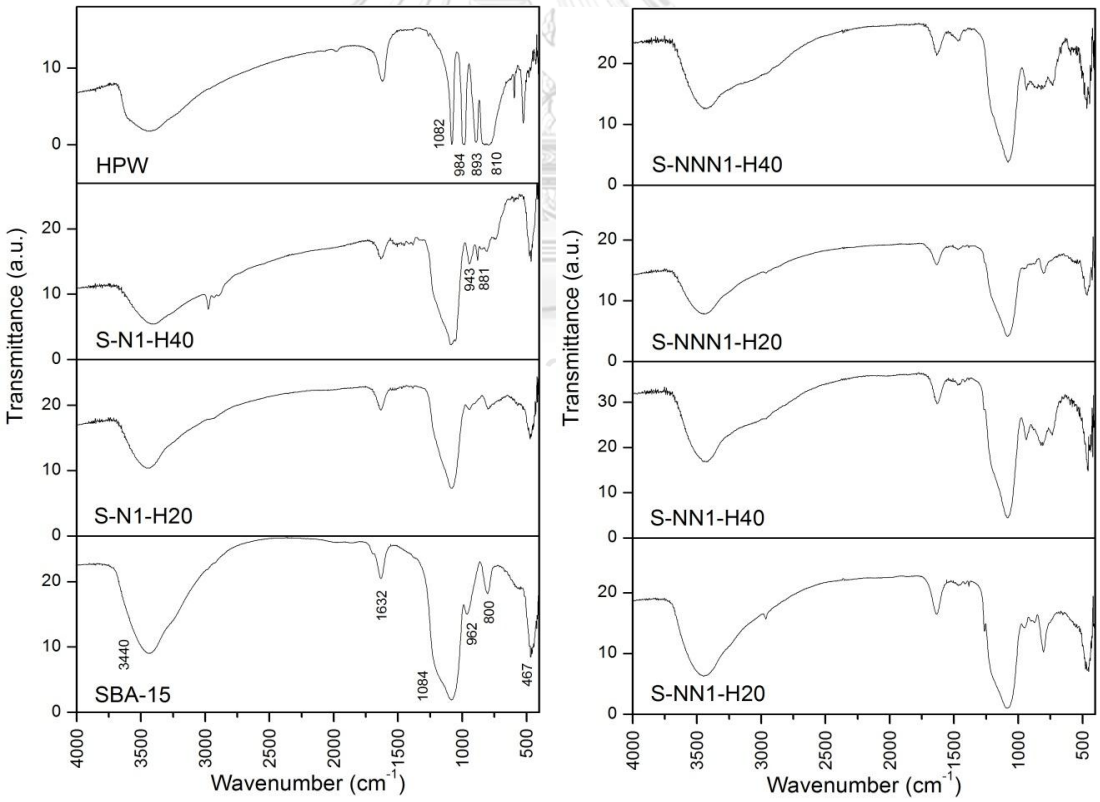

Figure 3.5 IR spectra of SBA-15, HPW, and acidified amine-functionalized SBA-15 materials.

3.1.4 Scanning electron microscope (SEM)

The morphologies of mesoporous silica SBA-15 and representative acidified amino-functionalized SBA-15 materials measured by SEM are shown in Fig. 3.6. The SEM images of acidified amino-functionalized SBA-15 (S-N1-H40, S-NN1-H40, and S-NNN1-H40) exhibited rope-like structure [97], similar to that of the parent SBA-15 material. This observation indicated that the presence of HPW and amino-organosilanes in the mesopores did not destroy the structure of the parent SBA-15.

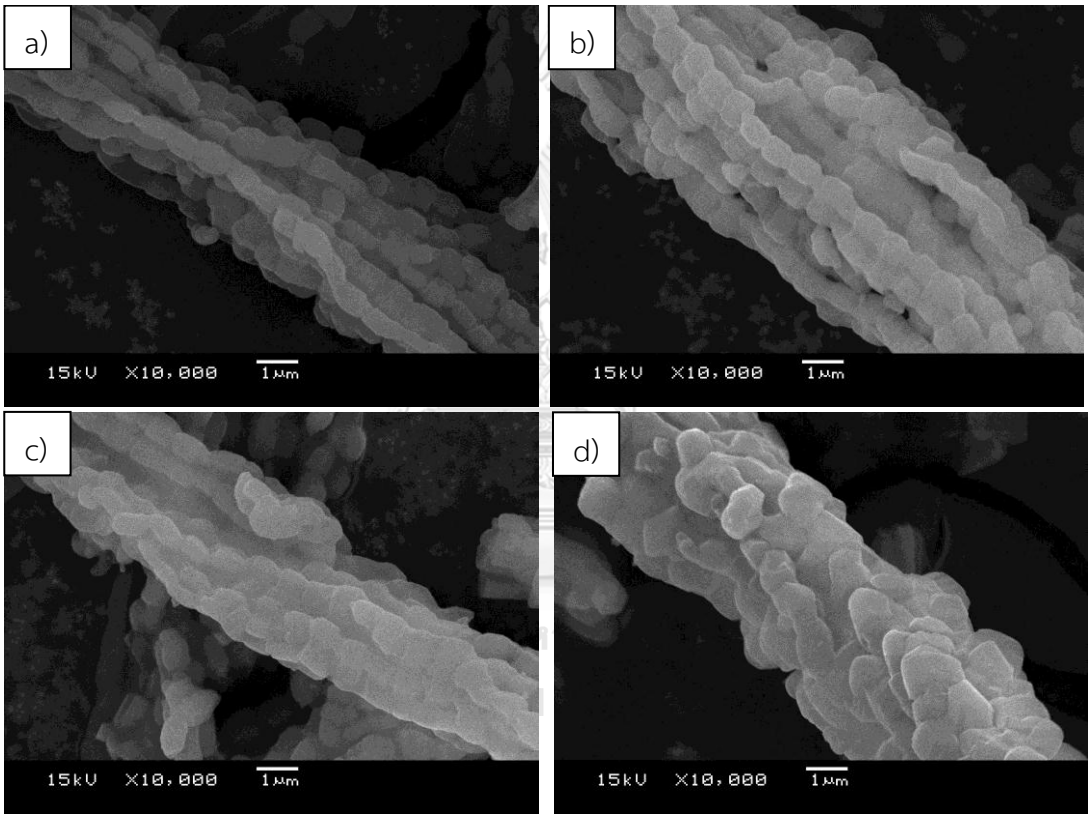

Figure 3.6 SEM images of (a) SBA-15, (b) S-N1-H40, (c) S-NN1-H40, and (d) S-NNN1-H40.

The weight ratios of Si/W in the synthesized materials were examined by scanning electron microscopy/energy dispersive X-ray spectroscopy (SEM/EDX) and the results are tabulated in Table 3.2. For all of the materials anchoring amino groups on SBA-15 surface prior to HPW addition, the weight ratios of Si/W in three random different regions were similar with the standard deviation (S.D.) ≤ 1.20, suggesting good dispersion of HPW species on the surface of the amine

functionalized SBA-15 supports. For the comparison purpose, the weight ratio of Si/W in S-H40 was also measured and the standard deviation was 4.13, implying that HPW species were not homogeneously dispersed into SBA-15 support. These findings indicated that amine functionalization of SBA-15 prior to the HPW immobilization helped the distribution of HPW on the surface of the support which would be beneficial when they were used as heterogeneous acid catalysts. Moreover, the average Si/W ratio of 0.77 for S-NN1-H40 of 0.77 measured by SEM/EDX was close to that of 0.82 measured by ICP-OES, confirming that HPW species were well-dispersed on the surface of amine functionalized materials.

Table 3.2 Weight ratios of Si/W in the synthesized materials using SEM/EDX by measuring at three different regions.

Materials	Weight ratio of Si/W			S.D.
	1	2	3	
S-N1-H20	1.81	2.07	2.40	0.29
S-N1-H40	0.83	0.87	0.87	0.02
S-NN1-H20	2.11	2.49	2.83	0.36
S-NN1-H40	0.77	0.77	0.77	0.00
S-NNN1-H20	3.74	5.70	5.92	1.20
S-NNN1-H40	0.61	0.61	0.61	0.00
S-H40	8.17	8.52	15.49	4.13

3.1.5 Transmission electron microscope (TEM)

TEM images of representative materials: pure SBA-15, S-NN1, and S-NN1-H40 are shown in Fig. 3.7. The arrangement of cylindrical channels in a uniform hexagonal structure was observed for pure SBA-15 and modified SBA-15 materials. The TEM results agreed well with the XRD results. Specifically, the structures of the modified SBA-15 materials were remained highly ordered with mesopore channels,

indicating that the introduction of amino-silane and HPW into the mesopore channels did not significantly alter the structure of SBA-15.

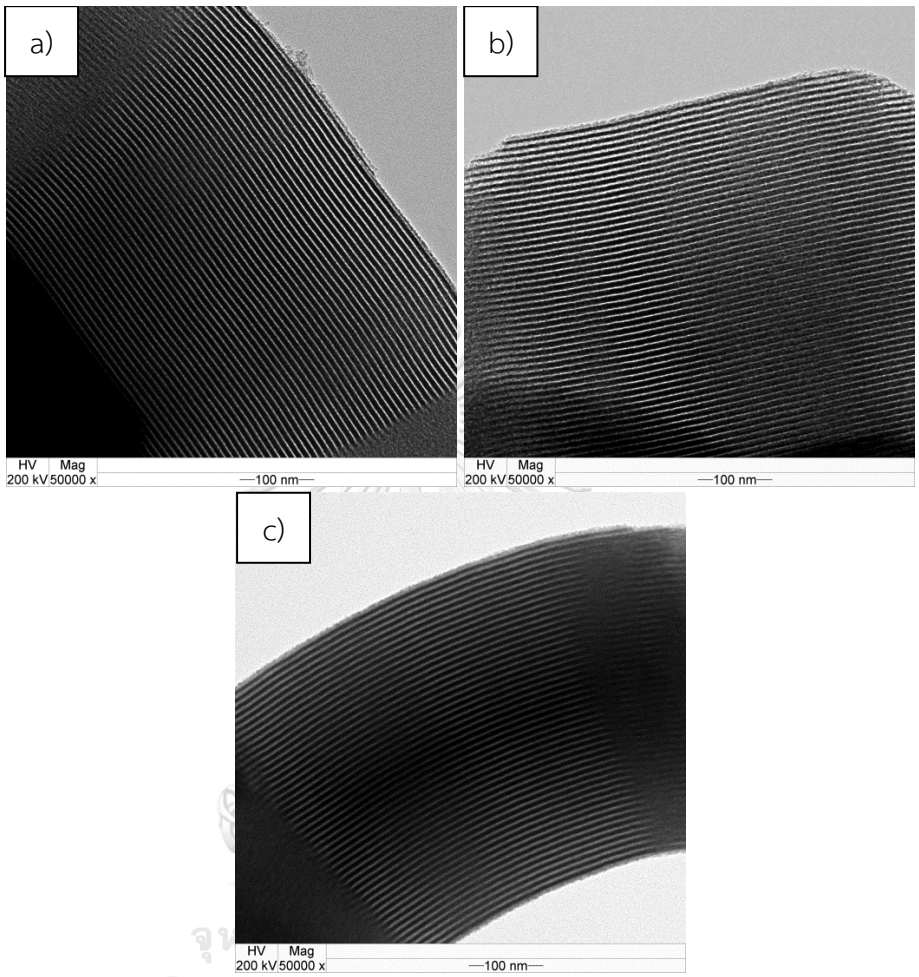

Figure 3.7 TEM images of (a) SBA-15, (b) S-NN1, and (c) S-NN1-H40.

3.1.6 Elemental analysis and acidity

The presence of amine groups can be determined by elemental analyzer. Table 3.3 shows the weight percentage of nitrogen atoms in the amine-functionalized SBA-15 materials. The results confirmed that the amine groups were successfully grafted on the surface of the supports in all samples. Additionally, the percentage of nitrogen atoms increased with increasing number of amine groups in the catalyst: 2.87%, 4.19%, and 6.58% for S-N1, S-NN1, and S-NNN1 samples, respectively. Furthermore, it was found that the weight percentage of nitrogen atoms corresponded to the acidity of the synthesized materials. Specifically, after

HPW immobilization, the materials containing higher number of amino groups were more protonated because amino groups were the primary sites to react with HPW. For comparison reasons, the acidity of S-H40 was also examined and found to be 0.30 mmole g^{-1} which was lower than that of S-N1-H40 (0.33 mmole g^{-1}), S-NN1-H40 (0.42 mmole g^{-1}), and S-NN1-H40 (0.49 mmole g^{-1}). This occurrence might be explained that $-NH_2$ groups have higher basicity than –OH groups, therefore, HPW could protonate the amine-functionalized SBA-15 materials more efficiently than S-H40.

Table 3.3 Elementals data and acidity of the synthesized materials.

Materials	%N (wt.%)[a]	acidity (mmole g^{-1})
S-N1	2.87	N/A
S-N1-H20	N/A	0.18
S-N1-H40	N/A	0.33
S-NN1	4.19	N/A
S-NN1-H20	N/A	0.24
S-NN1-H40	N/A	0.42
S-NNN1	6.58	N/A
S-NNN1-H20	N/A	0.31
S-NNN1-H40	N/A	0.49
S-H40	-	0.30

a measured by CHN analyzer

N/A = Not Available (not detected)

3.2 Catalytic activity of the synthesized materials

The synthesized SBA-15 mesoporous materials functionalized with different amino-organosilanes and acidified with tungstphosphoric acid were investigated for their catalytic activities in esterification of glycerol with oleic acid. The reaction with no catalyst was also performed for the purpose of comparison. In this study, the catalytic tests were divided into 7 parts:

(I) Effect of amino-organosilane types

(II) Effect of loading amount of tungstophosphoric acid (HPW)

(III) Effect of anchoring amino groups to SBA-15 surface prior to HPW addition

(IV) Reaction parameters affecting monoolein yield

(V) Catalyst reusability

(VI) Comparison of catalytic activity of the synthesized catalyst with commercial heterogeneous catalysts

(VII) Kinetic study

3.2.1 Effect of amino-organosilane types

Six acidified amine-functionalized SBA-15 materials were tested for their catalytic activities on the esterification of glycerol with oleic acid under the same conditions: glycerol/oleic acid molar ratio of 4:1, 160 °C, 5 h under nitrogen atmosphere, and 2.5 wt.% of catalyst loading. The conversions of oleic acid using modified catalysts are shown in Fig. 3.8. When the reaction was performed without the addition of a catalyst, the conversion of oleic acid could reach to 49% at 5 h, attributed to the ability of oleic acid as a self-catalyst for the esterification [71]. However, the oleic acid conversions were significantly higher for the reactions containing modified SBA-15 catalysts. Specifically, the conversions of oleic acid at 160°C for 5 h using S-N1-H20, S-NN1-H20, and S-NNN1-H20 catalysts were 76%, 80%, and 81%, respectively and a similar trend was also observed for 40% HPW containing catalysts: 81%, 95%, and 95% for S-N1-H40, S-NN1-H40, and S-NNN1-H40, respectively. As can be seen, S-NN1-H20 and S-NNN1-H20 catalysts exhibited similar oleic acid conversion but higher than S-N1-H20, suggesting that the degree of conversion increased with increasing acidity of catalysts (Table 3.3). However, acidity might not be the only factor affecting the conversion of oleic acid because even though S-NNN1-H20 contained more acid sites (0.31 mmole g^{-1}) than S-NN1-H20 (0.24 mmole g^{-1}), the conversions of oleic acid were similar. This observation might be explained that, besides catalyst acidity, pore size and surface area also had an

influence on the conversion. According to Table 3.1, the surface area of S-NN1-H20 (295 m^2 g^{-1}) was higher than that of S-NNN1-H20 (87 m^2 g^{-1}) and the pore diameter of S-NN1-H20 (7.05 nm) was also larger than that of S-NNN1-H20 (6.18 nm). Therefore, although S-NNN1-H20 contained more acid sites but it might be more difficult for the reactants to get to the reactive sites due to smaller surface area and pore size. Similar explanation could be also applied for a series of 40% HPW containing catalysts. These results suggested that the conversion of oleic acid depended on both the degree of acidity and pore characteristics of catalysts.

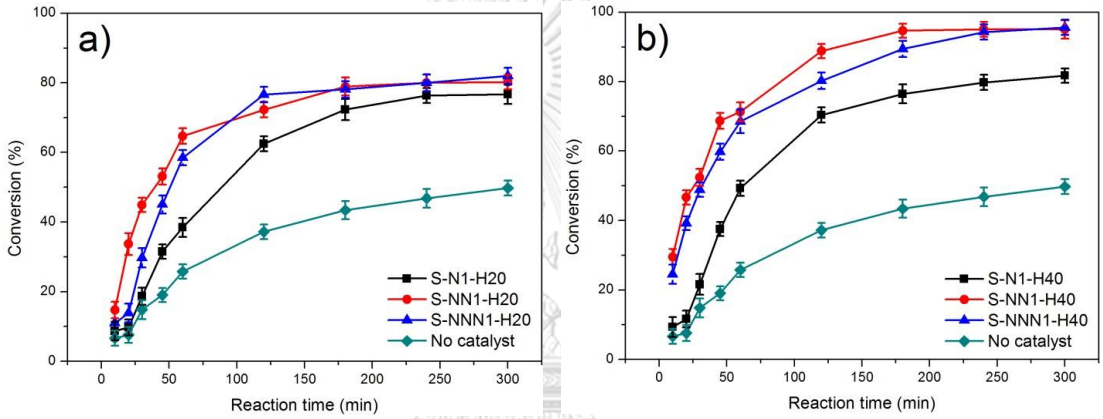

Figure 3.8 Effect of amino-organosilane types on conversion of oleic acid for a) 20 wt.% HPW containing catalysts and b) 40 wt.% HPW containing catalysts. Conditions: glycerol/oleic acid molar ratio of 4:1, 160 °C, 0-5 h, and 2.5 wt.% of catalyst loading.

In terms of yields of glyceride products obtained from esterification of glycerol with oleic acid using the prepared acid catalysts, the results are shown in Fig. 3.9. Among the 20% HPW containing catalysts, the yield of the desired monoolein product was highest when S-NN1-H20 was used. Similarly, among the 40% HPW containing catalysts, the use of S-NN1-H40 gave the highest monoolein yield. These findings could be resulted from both acidity and pore characteristics of the catalysts. For example, in a series of 40% HPW containing catalysts, S-N1-H40, which was less acidic than S-NN1-H40 and S-NNN1-H40, gave less oleic acid conversion and less monoolein yield. However, S-NN1-H40 and S-NNN1-H40, which gave the same oleic acid conversion, gave significantly different monoolein yield. This occurrence was likely due to their different surface areas and pore sizes. In

other words, the smaller surface area and pore size of S-NNN1-H40, as compared to those of S-NN1-H40, might block some reactants to diffuse and react in the pores. Therefore, the reaction might partly occur at the external surface or around the mouth of the pores, leading to less selective toward monoolein production. Instead, bulkier diolein and triolein products were formed. After ~2-3 h of reaction, monoolein yield reached the maximum for all catalysts. However, the monoglyceride yield did not decrease after reaching the maximum points even though the yields of diolein and/or triolein kept increasing over time, which was similar to another work reported by Hermida et al. [91]. This finding indicated that most of diolein and triolein were likely to be directly produced from esterification of glycerol and oleic acid but not from the esterification reaction of the generated monoglyceride and oleic acid. These results led to a proposed reaction pathway as illustrated in Scheme 3.1. The corresponding nucleophilic substitution mechanism to produce monoolein is shown in Scheme 3.2.

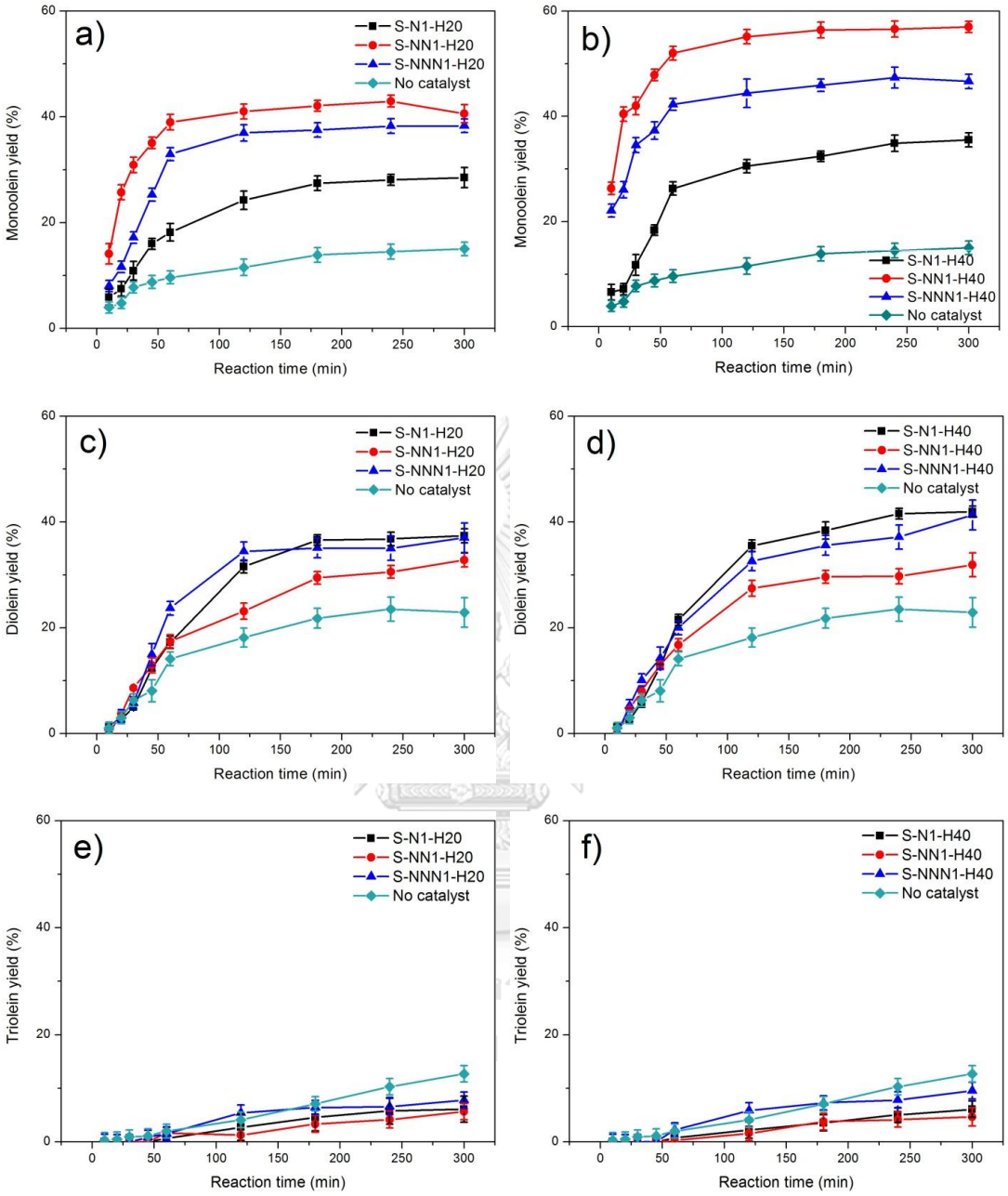

Figure 3.9 Effect of amino-organosilane types on yields of glyceride products. Conditions: glycerol/oleic acid molar ratio of 4:1, 160 °C, 0-5 h, and 2.5 wt.% of catalyst loading.

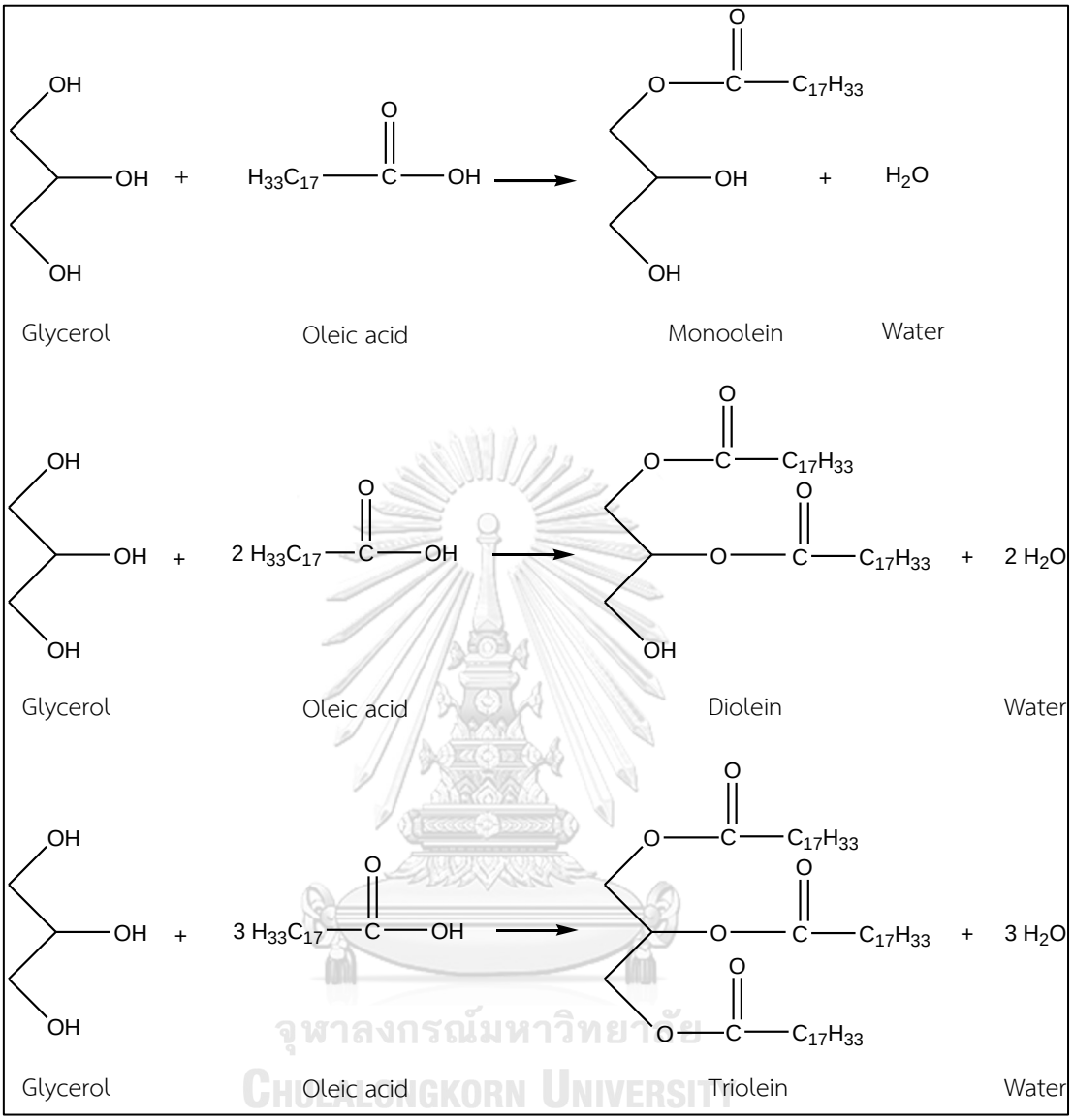

Scheme 3.1 The proposed reaction pathway of esterification of glycerol with oleic acid using acidified amine-functionalized SBA-15 catalysts.

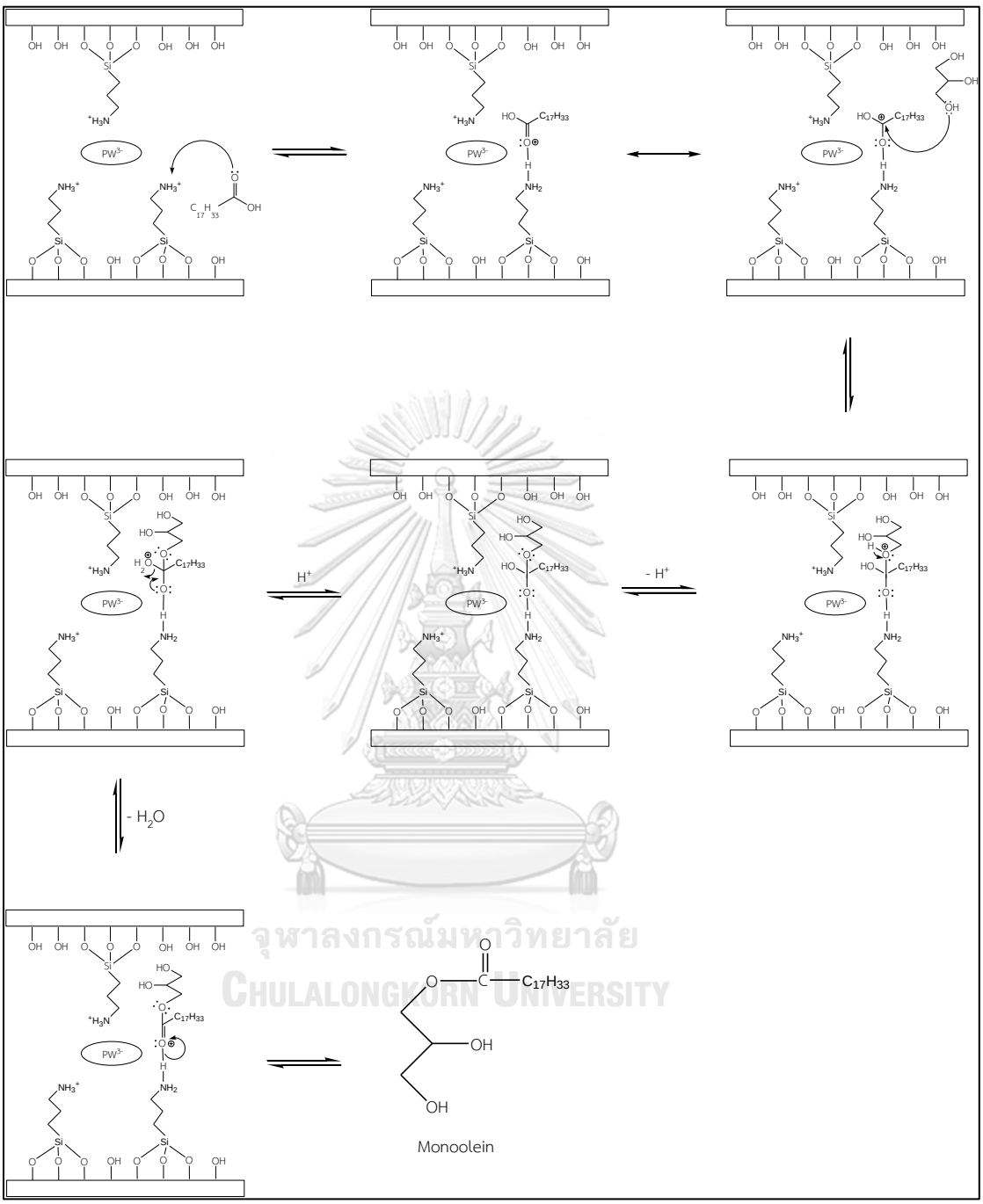

Scheme 3.2 The proposed nucleophilic substitution mechanism to produce monoolein by esteridication of glycerol with oleic acid.

3.2.2 Effect of loading amount of tungstophosphoric acid (HPW)

Effect of HPW loadings (20 wt.% and 40 wt.%) into the amine functionalized SBA-15 materials on catalytic activity of esterification of glycerol with

oleic acid were investigated under the conditions of glycerol/oleic acid molar ratio of 4:1, 160 °C, 0-5 h, and 2.5 wt.% of catalyst loading. S-NN1-H20 and S-NN1-H40 catalysts were selected to investigate the effect of different HPW loadings on oleic acid conversion and glyceride yields as shown in Fig. 3.10. The results showed that the reaction with S-NN1-H40 catalyst performed more efficiently than S-NN1-H20 in terms of both conversion and monoglyceride yield. This finding could be explained by the acidity of the catalysts. As reported in Table 3.3, the acidities of S-NN1-H20 and S-NN1-H40 were 0.25 and 0.38 mmole g^{-1}, respectively. This information indicated that the catalytic activity was increased with the increase of HPW loading, likely due to the increasing number of acidic sites. As compared to the reaction with no catalyst added, the reactions with synthesized heterogeneous catalysts led to significantly higher oleic acid conversion and monoolein yield, suggesting that the reactions that mainly occurred in the mesopores of the synthesized S-NN1-H20 and S-NN1-H40 catalysts led to high selectivity towards monoolein product. Because the reaction with no catalyst occurred in homogeneous solution, less selectivity towards monoolein and higher selectivities towards bulky dioein and triolein were observed. However, the selectivity towards monoolein using S-NN1-H20 and S-NN1-H40 heterogeneous catalysts was not significantly different, which is likely due to their similar pore size of 7.05 nm.

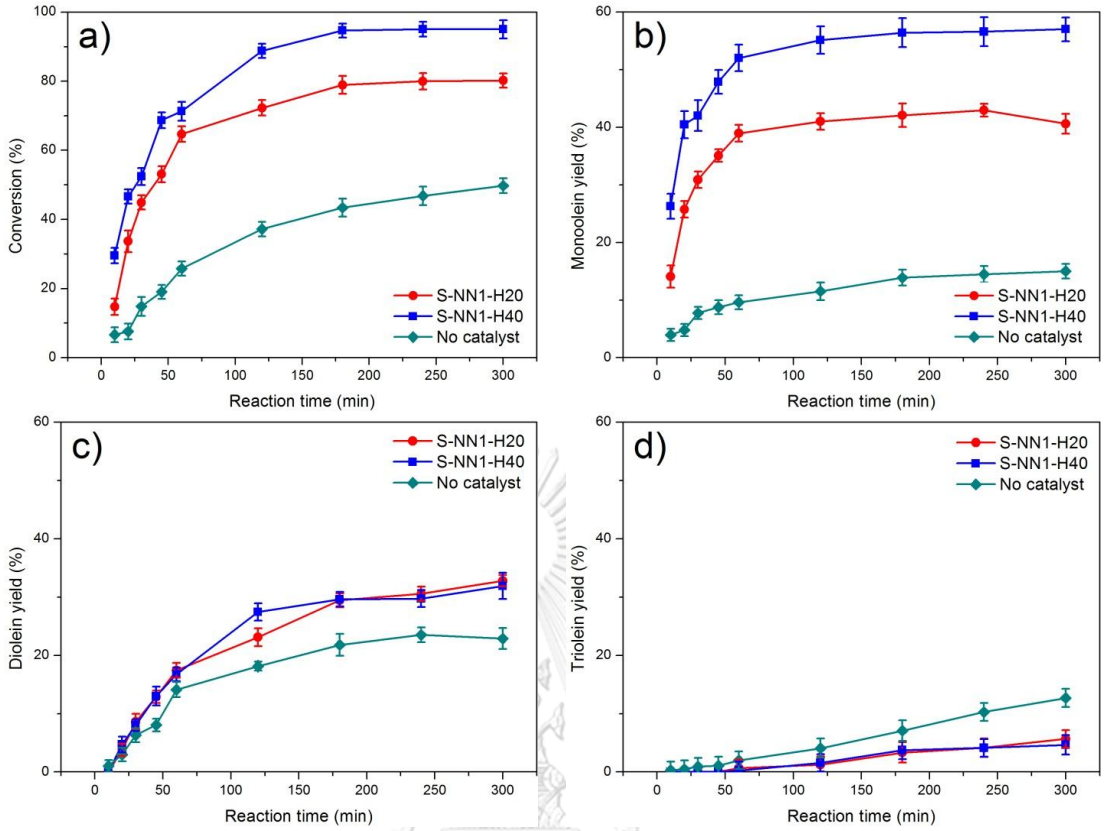

Figure 3.10 Effect of HPW loading on conversion of oleic acid (a) and glyceride yields (b, c, d). Conditions: glycerol/oleic acid molar ratio of 4:1, 160 °C, 0-5 h, and 2.5 wt.% of catalyst loading.

3.2.3 Effect of anchoring amino groups to SBA-15 surface prior to HPW addition

In order to investigate the role of anchoring amino groups to the surface of SBA-15 prior to HPW addition, a catalyst containing no amino groups was also synthesized for the purpose of comparison. In this part, the catalytic performance of 40 wt.% HPW immobilized on amine-functionalized SBA-15 (S-N1-H40, S-NN1-H40, S-NNN1-H40) were studied and compared to that of 40 wt.% HPW immobilized on SBA-15 (S-H40). As shown in Fig. 3.11, the use of S-H40 gave similar oleic acid conversion to that of S-N1-H40 but lower than that of S-NN1-H40 and S-NNN1-H40. It might be explained by the acidity of catalysts; *i.e.*, S-H40 and S-N1-H40 had similar acidity (0.30 mmole g^{-1} for S-H40 and 0.33 mmole g^{-1} for S-N1-H40) which were less than that of S-NN1-H40 (0.42 mmole g^{-1}) and S-NNN1-H40 (0.49 mmole g^{-}

[1]). In terms of glyceride yields, the use of S-H40 less favored in monoolein production, as compared to that of HPW immobilized on amine-functionalized SBA-15. This finding could be because the pore diameter of S-H40 (9.23 nm) might be too large to selectively form only monoolein product because diolein and especially triolein were also obtained when S-H40 was used as a catalyst. These results strongly suggested that in order to obtain high yield of monoolein, both acidity and pore characteristics of catalysts were important factors to be considered.

Based on the experimental results of oleic acid conversion and monoolein yield from sections 3.2.1-3.2.3, the most effective catalyst in this study was S-NN1-H40 catalyst, therefore, it was used as a representative catalyst to be further studied in the next sections.

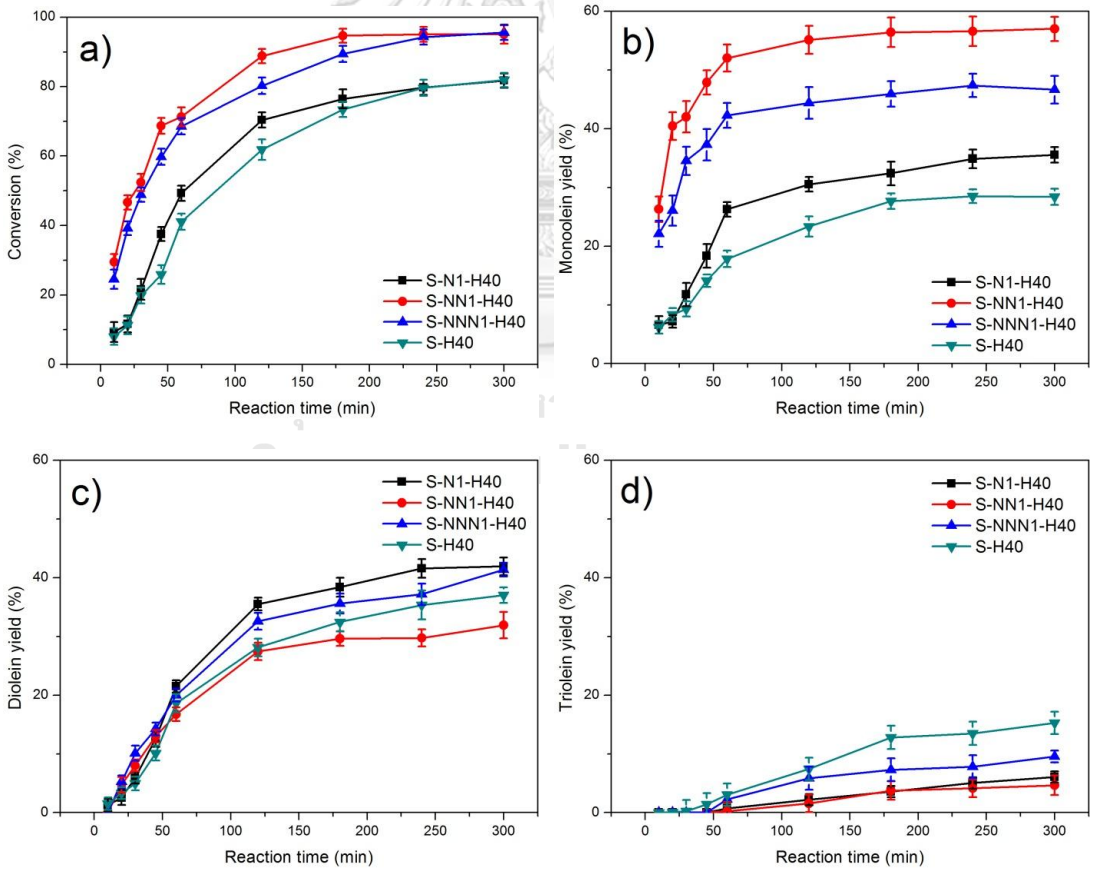

Figure 3.11 Effect of anchoring amino groups to SBA-15 surface prior to HPW addition on conversion of oleic acid (a) and glyceride yields (b, c, d). Conditions: glycerol/oleic acid molar ratio of 4:1, 160 °C, 0-5 h, and 2.5 wt.% of catalyst loading.

3.2.4 Reaction parameters affecting monoolein yield

3.2.4.1 Effect of reaction temperature

The effect of reaction temperature on oleic acid conversion and yield of glyceride products are shown in Fig. 3.12. The reaction temperature was studied in the range of 120 °C to 180 °C for 0-3 h with glycerol/oleic acid molar ratio of 4:1, and 2.5 wt.% of S-NN1-H40 catalyst loading. At the initial stage, when the reaction temperature was increased from 120 °C to 180 °C, oleic acid conversion and monogleceride yield were significantly increased. These results suggested that kinetic energy of the reactants increased with the increase of the reaction temperature, resulting in the improvement of the interaction between glycerol and oleic acid starting materials [98]. However, the oleic acid conversion and monoolein yield were increased gradually during the 2-3 h of reaction time probably due to the reaction was close to reach the equilibrium. However, although rate of reactions increased with increasing the reaction temperature, the use of high temperature resulted in an undesired change in color of the glyceride products (Fig. 3.13) [99]. Obviously, the color of the reaction mixture was darker when the reaction was performed at 180 °C, as compared to those performed at 120-160 °C. In addition, the use of high temperature also led to increase in diolein and triolein yields due to higher energy was required to overcome the energy barrier and steric hindrance to form diolein and triolein [29]. Therefore, based on the above reasons, the reaction temperature of 160 °C was chosen for further studies.

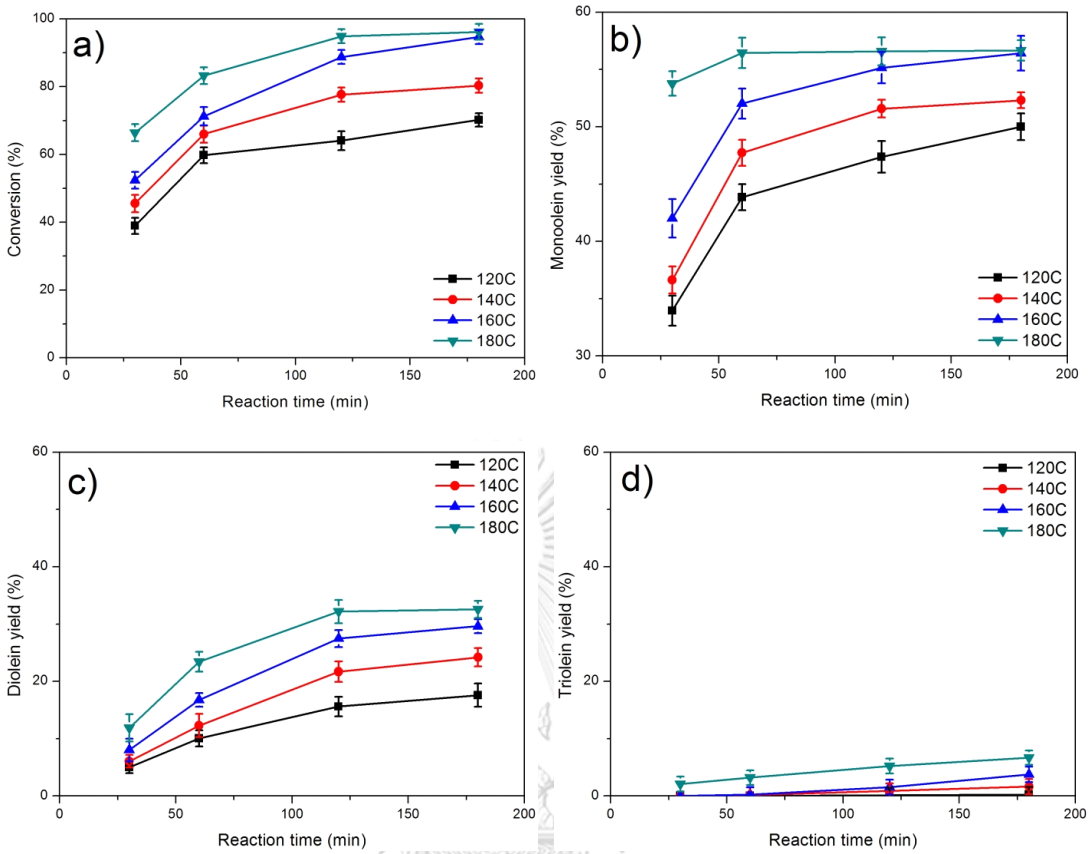

Figure 3.12 Effect of reaction temperature (120 °C - 180 °C) on conversion of oleic acid (a) and glyceride yields (b, c, d). Conditions: glycerol/oleic acid molar ratio of 4:1, 0-3 h, and 2.5 wt.% of S-NN1-H40 catalyst loading.

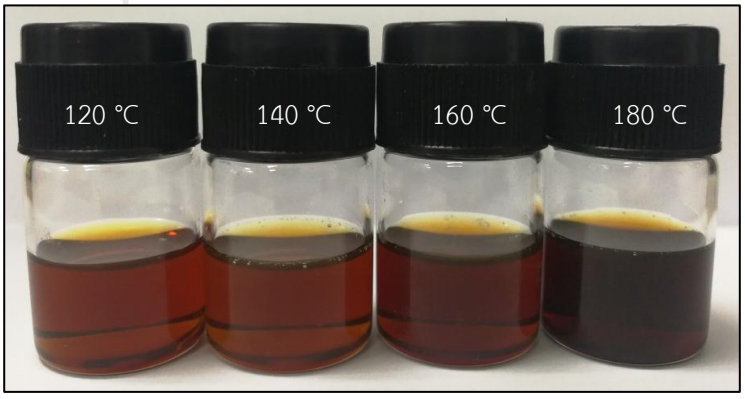

Figure 3.13 Colors of reaction mixtures of the 3 h esterification reactions using different temperatures.

3.2.4.2 Effect of reactants ratio

The effect of glycerol/oleic acid molar ratio on oleic acid conversion and yield of glyceride products are shown in Fig. 3.14. The glycerol:oleic acid molar ratios of 1:1, 2:1, 4:1 and 6:1 were studied at 160 °C, 0-3 h, and 2.5 wt.% of S-NN-H40 catalyst loading. The results showed that oleic acid conversion was enhanced when the molar ratio of glycerol to oleic acid was increased from 1:1 to 4:1. Based on Le Chatelier's Principle, an excess amount of glycerol was needed in order to shift the reaction equilibrium to the right-hand side for a higher formation of the glyceride products. Therefore, the conversion of oleic acid was increased by increasing the molar ratio of glycerol/oleic acid as expected. However, when the molar ratio was increased to 6:1 the conversion slightly dropped probably because too much amount of glycerol might hinder the product formation by the diffusion of starting materials into the mesopores of the catalyst [100]. Considering the yields of glyceride products, monoglyceride yield was significantly increased with increasing molar ratio of glycerol to oleic acid from 1:1 to 1:4 while diglyceride and triglyceride yields were decreased. These results might be explained by the fact that the increase in glycerol/oleic acid molar ratio increased the opportunity for glycerol to interact with oleic acid to form monoolein. However, when the glycerol/oleic acid molar ratio was increased to 6:1, monoolein and diolein yields did not increased while triglyceride yield slightly increased over time. This finding might be explained that the presence of a large amount of reactants could hinder the diffusion of starting materials into the pore channels of the catalyst, hence the reaction partly occurred at the external surface of the catalyst. Consequently, this led to the increase in the formation of bulky triolein product when a 6:1 molar ratio was employed. Therefore, based on the above reasons, the glycerol/oleic acid molar ratio of 4:1 was chosen for further studies.

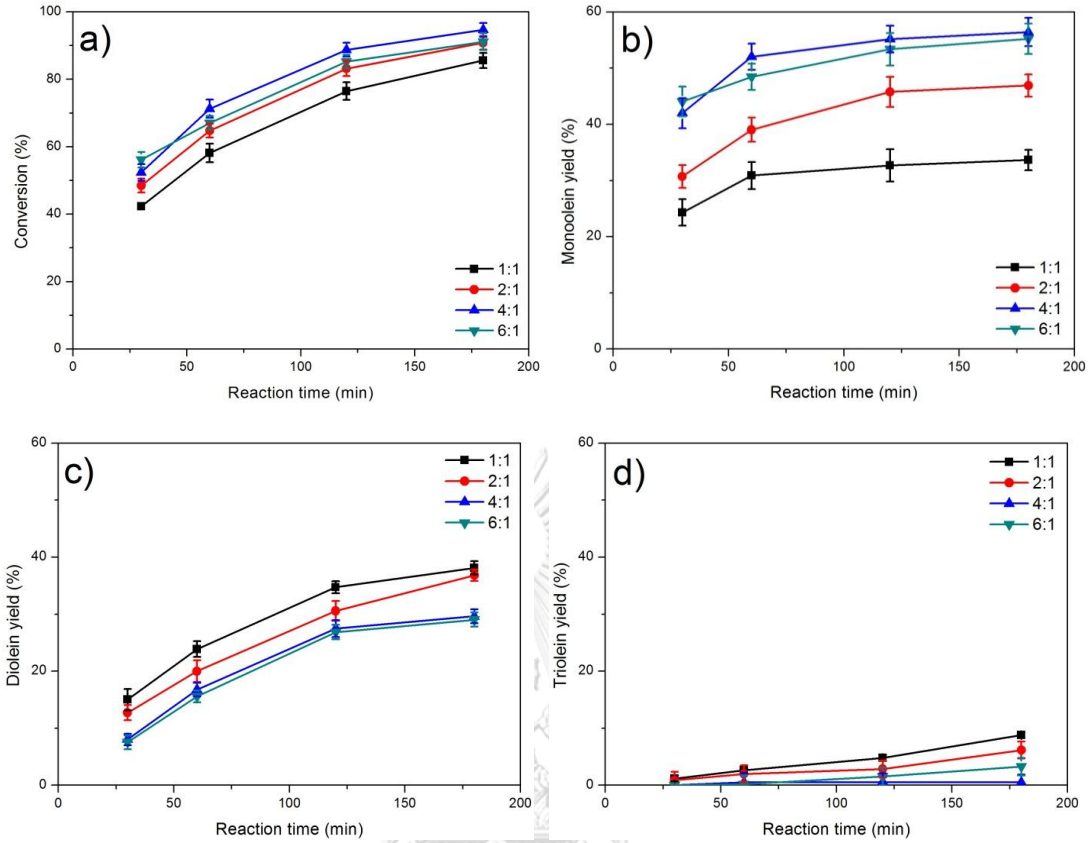

Figure 3.14 Effect of glycerol:oleic acid molar ratio (1:1, 2:1, 4:1, and 6:1) on conversion of oleic acid (a) and glyceride yields (b, c, d). Conditions: 160 °C, 0-3 h, and 2.5 wt.% of S-NN-H40 catalyst loading.

3.2.4.3 Effect of catalyst loading

The effect of catalyst loading on oleic acid conversion and yield of glyceride products are shown in Fig. 3.15. The S-NN1-H40 catalyst loadings of 0, 1.5, 2.5, and 3.5 wt.% were studied at 160 °C, 0-3 h, and glycerol/oleic acid molar ratio of 4:1. The results showed that oleic acid conversion was increased with the increase of catalyst loading from 1.5 to 2.5 wt.%, likely due to the increasing number of acidic sites available for the reaction. However, when the catalyst loading was increased to 3.5 wt.%, no further enhancement in oleic acid conversion was observed. This occurrence could be explained that the reaction with 3.5 wt.% of the catalyst contained excess acidic sites than actually required by the starting materials under the conditions used [91]. Interestingly, the reaction without catalyst could

reach 49% conversion at 5 h, attributed to the ability of oleic acid as a self-catalyst for the esterification. However, the reaction with no catalyst gave only 15% yield of monoolein while diglyceride and triglyceride yields were 22% and 12%, respectively. The lower monoglyceride yield, compared to diglyceride yield, obtained from the reaction without catalyst might be because the reaction occurred in the bulk solution, not in the mesopores of a heterogeneous catalyst, leading to poor selectivity towards monoolein product. In other words, shape and pore size of the porous heterogeneous catalyst, where the reaction occurred, might play an important role for the selectivity of the glyceride products. Considering the yields of glyceride products in the heterogeneous catalyst-containing reactions, a similar trend as the conversion was observed. In this condition, the yields of glyceride products were increased with increasing catalyst from 1.5 to 2.5 wt.% but no further enhancement in glyceride yields was observed. Therefore, based on the above reasons, the catalyst loading of 2.5 wt.% was chosen for further studies.

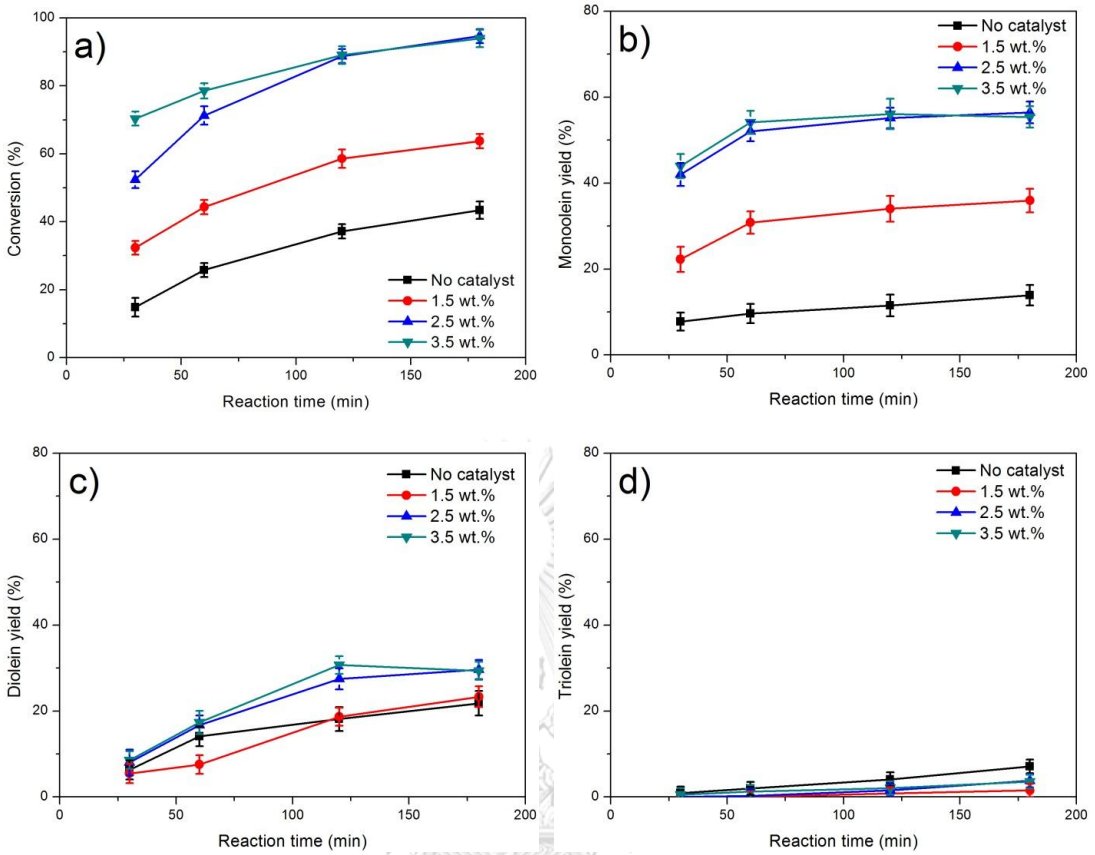

Figure 3.15 Effect of S-NN1-H40 catalyst loading (0, 1.5, 2.5, and 3.5 wt.%) on conversion of oleic acid (a) and glyceride yields (b, c, d). Conditions: 160 °C, glycerol/oleic acid molar ratio of 4:1, and 0-3 h.

3.2.5 Catalyst reusability

Reusability study of the S-NN1-H40 and S-H40 catalysts were carried out by repeating the esterification of oleic acid and glycerol for 6 cycles. As shown in Fig. 3.16, no significance in catalytic activity loss was observed in the first three cycles for both catalysts (90.7-91.4%, and 69.9-71.5% conversion for S-NN1-H40 and S-H40 catalysts, respectively). After the 6^{th} cycle, the conversion was dropped only 7% for the S-NN1-H40 containing reaction but dropped 16% for the S-H40 containing reaction. This finding could be explained that, for the S-H40 catalyst, the H-bonding between HPW and the silanol groups (≡Si-OH) on the surface of SBA-15 was not as strong as the interaction between HPW and the amino groups (-NH_2) in the S-NN1-

H40 catalyst [59, 64]. Consequently, the active sites in S-H40 leached out to the reaction mixture more than that in S-NN1-H40, *i.e.*, 0.03 and 0.22 wt.% leaching of tungsten (W) for S-NN1-H40 and S-H40 catalysts, respectively, as examined by ICP-OES. These results confirmed the high stability of S-NN1-H40, in which amino groups were grafted on the surface of SBA-15 before firmly anchoring HPW to amino groups *via* ionic bonding, leading to high dispersion of HPW on the modified support, minimal leaching, and boosting the reusability of the catalyst [64].

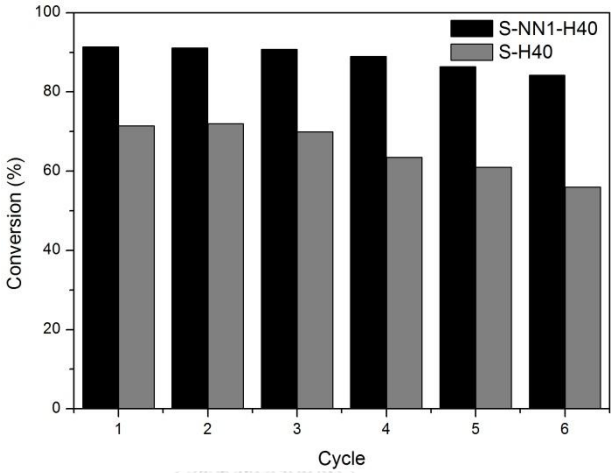

Figure 3.16 Reusability of S-NN1-H40 and S-H40 catalysts in esterification of glycerol with oleic acid. Conditions: 160 °C, glycerol/oleic acid molar ratio of 4:1, 3 h, and 2.5 wt.% of catalyst loading.

3.2.6 Comparison of catalytic activity of the synthesized catalyst with commercial heterogeneous catalysts

The S-NN1-H40 catalyst, which was the best catalyst in this study, was compared its catalytic activity for esterification of oleic acid and glycerol with other three commercial catalysts: H-BEA zeolite, ZSM-5 zeolite and Amberlyst-15. The catalytic activity in terms of oleic acid conversion of S-NN1-H40 and other commercial catalysts are shown in Fig. 3.17. The results showed that S-NN1-H40 provided 91% conversion which was significantly higher than that of H-BEA zeolite (73%), ZSM-5 zeolite (70%), and Amberlyst-15 (50%). In case of H-BEA and ZSM-5 zeolites, both of them had smaller pore sizes than S-NN1-H40 (0.66 nm [101], 0.63 nm [102], and 7.05 nm for H-BEA, ZSM-5, and S-NN1-H40, respectively). Therefore,

the use of both zeolites with micropore sizes could retard the diffusion of the reactants into their micropores. Considering the use of Amberlyst-15, the lowest oleic acid conversion was obtained probably because Amberlyst-15, which had low thermal stability, was decomposed at ~120 ℃, resulting in the loss of active sites of the catalyst and poor catalytic activity [103].

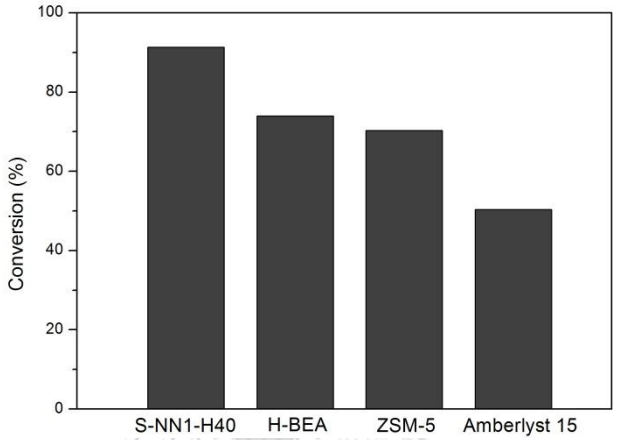

Figure 3.17 Oleic acid conversion of esterification of oleic acid and glycerol using S-NN1-H40 and other three commercial catalysts. Conditions: 160 ℃, glycerol/oleic acid molar ratio of 4:1, 3 h, and 2.5 wt.% of catalyst loading.

3.2.7 Kinetic study

The kinetic study for esterification of glycerol with oleic acid using the S-NN1-H40 catalyst was carried out at 120 ℃ - 160 ℃, 0.5-3 h, glycerol/oleic acid molar ratio of 4:1, and 2.5 wt.% of S-NN1-H40 loading. According to the first order kinetic equations as given in Eqs. (1)-(3), the plot of ln (C_0/C) and reaction time (t) would give a linear relationship. The regression coefficients (R^2) of the straight lines exhibited good fits to first order kinetics (Fig. 3.18) [62] and these results agreed well with some previously reported works [55, 62].

From the first order kinetic equation [104]:

$$\text{Rate} = \frac{-d[C]}{dt} = k[C] \quad (1)$$

This can further be arranged into y = mx + b form:

$$\ln[C] = -kt + \ln[C]_0 \quad (2)$$

Now, recall from the laws of logarithms that:

$$\ln\frac{[C]_o}{[C]} = kt \quad (3)$$

Therefore; slope = k

Where k = first-order rate constants (min^{-1})

$[C]_0$ = concentration of oleic acid at time 0 (mole L^{-1})

$[C]$ = concentration of oleic acid at time t (mole L^{-1})

t = reaction time (min)

The rate constants (k) at various reaction temperatures were calculated from the slopes of kinetic first-order plots and are listed in Table 3.4. When the reaction temperature was increased from 120 to 160 °C, the kinetic energy of the reactants was significantly increased due to the rate constants of the reactions were increased from 3.90 x 10^{-3} to 14.6 x10^{-3} min^{-1}. This result suggested that oleic conversion increased with the increasing of the reaction temperature because the reactants had higher kinetic energy at high reaction temperature [91]. However, when the temperature was increased from 160 °C to 180 °C, the rate constant was insignificantly different because oleic conversion at both reaction temperatures were not much different. In addition, the rate constants of the reactions using the synthesized catalysts were investigated to confirm their catalytic activities at the optimum conditions as shown in Table 3.5. The results show that the rate constant of the reaction using S-NN1-H40 was 18.5 x 10^{-3} min^{-1}, which was the highest value as compared to that of the other synthesized catalysts. Therefore, the results confirm that the catalytic activity of the reaction depended on both of acidity and pore characteristics of the catalysts.

From the rate constants of the reactions using S-NN1-H40 catalyst at different temperatures, ln(k) versus 1/T was plotted to determine activation energy (Ea) of the reaction by the Arrhenius equation as given in Eq. (4) (Fig. 3.19).

From the Arrhenius equation [55]:

$$k = Ae^{(-Ea/RT)} \quad (4)$$

This can further be arranged into y= mx + b form:

$$\ln(k) = \left(\frac{-Ea}{RT}\right) + \ln(A) \quad (5)$$

Therefore; slope = $\left(\frac{-Ea}{R}\right)$

Where *k* = rate constant (min^{-1})

Ea = activation energy (kJ $mole^{-1}$)

A = pre-exponential factor

R = gas constant (8.314 J K^{-1} mol^{-1})

T = reaction temperature (Kelvin)

The value of activation energy of esterification of glycerol with oleic acid using S-NN1-H40 catalyst was 35.45 kJ mol^{-1}. Given that if the reaction rate is diffusion limited/mass transfer limited, the *Ea* value for diffusion limited reactions is 10–15 kJ $mole^{-1}$ whereas if the reaction rate is controlled by the chemical step where the catalyst is being used to its maximum capacity, the *Ea* value is normally higher than 25 kJ $mole^{-1}$[59, 62]. Therefore, because the activation energy in this study was 35.45 kJ $mole^{-1}$, the reaction rate was likely to be governed by the chemical step.

Table 3.4 Rate constants for the first-order kinetic model.

Temperature (°C)	Rate constant (k) x 10^{-3} (min^{-1})
120	3.90
140	6.50
160	14.6
180	14.5

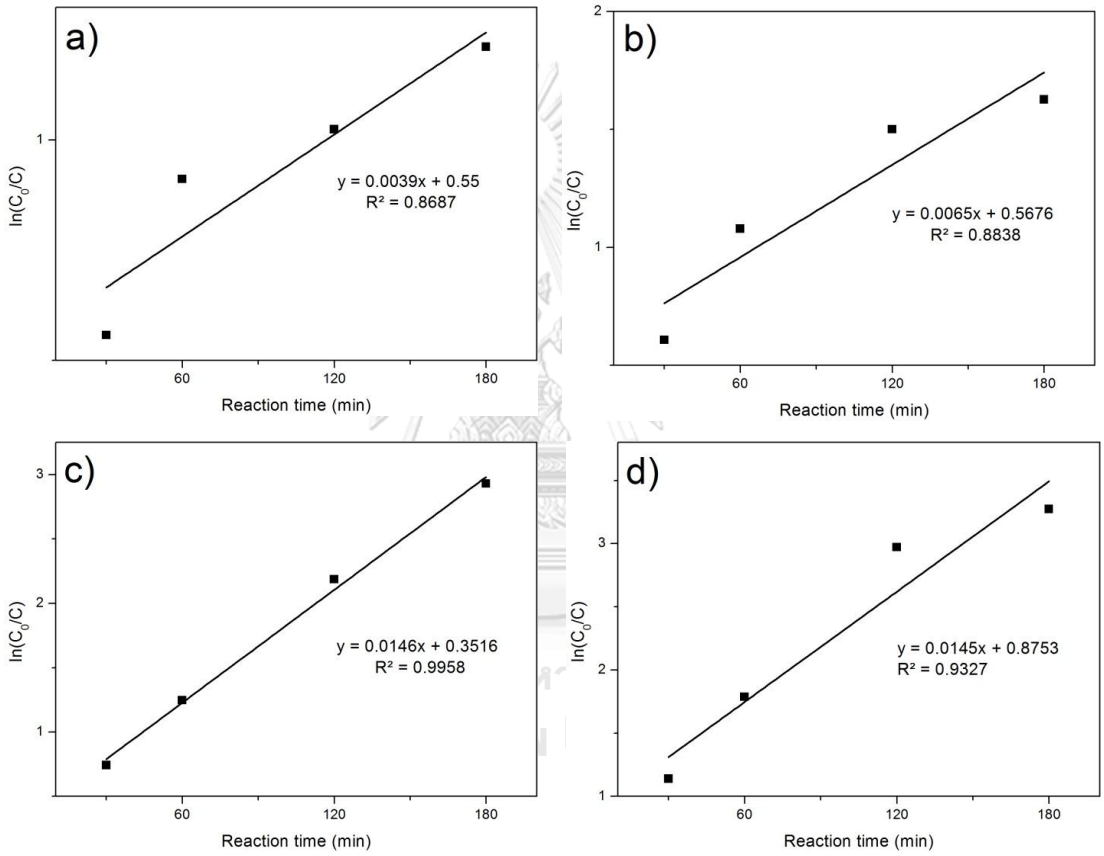

Figure 3.18 Kinetic first-order plots for esterification of glycerol with oleic acid using the S-NN1-H40 catalyst at the reaction temperature of a) 120 °C, b) 140 °C, c) 160 °C, and d) 180 °C. Conditions: glycerol/oleic acid molar ratio of 4:1, 0.5-3 h, and 2.5 wt.% of catalyst loading.

Table 3.5 Rate constants for esterification of glycerol with oleic acid.

Materials	Rate constant (k x 10^{-3}) (min-1)
S-N1-H20	8.6
S-NN1-H20	16.7
S-NNN1-H20	16.0
S-N1-H40	12.3
S-NN1-H40	18.5
S-NNN1-H40	17.8
S-H40	8.7

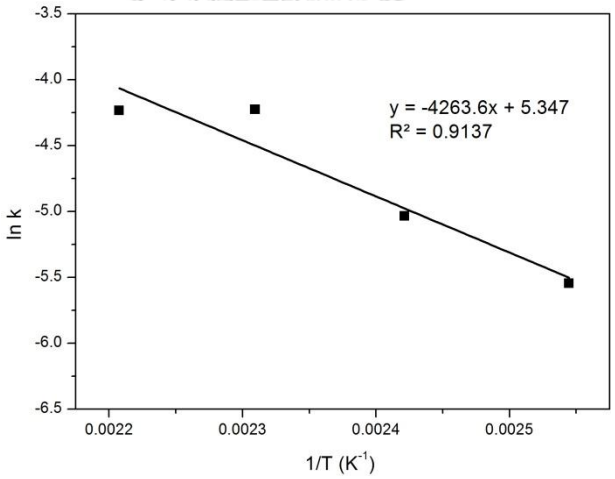

Figure 3.19 Arrhenius plot of ln(*k*) versus 1/*T* of esterification of glycerol with oleic acid using S-NN1-H40 catalyst. Conditions: 120 °C - 160 °C, glycerol/oleic acid molar ratio of 4:1, 3 h, and 2.5 wt.% of catalyst loading.

CHAPTER IV
CONCLUSIONS

The mesoporous SBA-15 material was synthesized *via* the hydrothermal method and further functionalized with three types of amino-organosilanes: APTES (N), AAPTMS (NN), and DETTMS (NNN) using the post-grafting method. Then, 20 wt.% and 40 wt.% of Keggin-type tungstophosphoric acid (HPW) was successfully anchored on the surface of each synthesized amine-functionalized SBA-15 material using the impregnation method. Six modified SBA-15 materials including S-N1-H20, S-NN1-H20, S-NNN1-H20, S-N1-H40, S-NN1-H40, and S-NNN1-H20 were obtained.

The characterization results showed that the synthesized materials remained highly ordered with mesopore channels and exhibited rope-like structure, similar to that of the parent SBA-15. These results indicated that the mesoporous structure of the support was not destroyed after the modification. The surface areas and pore diameters of the synthesized materials were in the range of 55 to 299 $m^2 g^{-1}$ and of 6.18 to 7.05 nm, respectively. The acidity of all materials was in the range of 0.18 to 0.49 mmole g^{-1}. In addition, the results indicated that the acidity of the synthesized materials was proportional to the number of amine groups in the amino-organosilanes employed.

The six synthesized materials were used as catalysts to evaluate their catalytic activities for the esterification reaction of glycerol with oleic acid to produce monoolein under the following reaction condition: glycerol/oleic acid molar ratio of 4:1, 160 °C, 3 h, and 2.5 wt.% of catalyst loading. The main findings were as follows:

1. The conversion of oleic acid and the yield of monoolein significantly depended on both of the degree of acidity and pore characteristics of catalysts. The use of S-NN1-H40 catalyst gave the highest monoolein yield probably because it had the most suitable acidity (0.42 mmole g^{-1}) and pore characteristics (surface area,

pore volume, and pore diameter of S-NN1-H40 catalyst were 177 $m^2 g^{-1}$, 0.31 $cm^3 g^{-1}$, and 7.05 nm, respectively). Although the S-NNN1-H40 catalysts had the highest acidity compared to all synthesized catalysts, it was not the catalyst that gave the highest monoolein yield probably because the size of the NNN aminosilane was so bulky that some reactants could not easily diffuse and react in the pores.

2. Functionalization of SBA-15 with aminosilanes on the surface of SBA-15 prior to HPW addition (S-NN1-H40), as compared to the catalyst containing no amino groups (S-H40), assisted the distribution of HPW throughout the support, leading to the improved efficiency as a heterogeneous acid catalyst.

3. The catalytic activity of synthesized S-NN1-H40 catalyst showed higher activity than some commercial heterogeneous catalysts: H-BEA zeolite, ZSM-5 zeolite, and amberlyst-15.

4. For the reusability study, the S-NN1-H40 catalyst showed a good maintenance of activity in the first six cycles without a significant loss in catalytic activity, which was superior to that of the S-H40 catalyst. The better stability of the S-NN1-H40 catalyst can be attributed to the strong interaction between the amino groups on the surface of SBA-15 and HPW.

5. The kinetic study showed that the esterification of glycerol with oleic acid using the S-NN1-H40 catalyst exhibited the first-order rate law with the rate constant of 14.6 x 10^{-3} min^{-1} at 160 °C. From the Arrhenius plot, the value of activation energy (*Ea*) was found to be 35.45 kJ mol^{-1}, suggesting that the reaction rate was governed by the chemical step.

Suggestions for future work

1. Surface modification of protonated amine-functionalized materials with hydrophobic groups in order to improve the reusability of catalysts caused by the leaching problem.

2. Study of shape and size selectivity of the modified porous materials on the production of other value-added chemicals in other reactions that require acid catalysts.

REFERENCES

[1] How do Catalysts work [Online]. Available from: http://www.4college.co.uk/as/atm/catalysts.php [2017, Oct 21]

[2] Reaction Rates: Collision theory, measurement and mechanism [Online]. Available from: https://archive.cnx.org/contents/a433fc1b-e473-4eeb-9f3b-46e34d25c0d2@1/reaction-rates-collision-theory-measurement-and-mechanism [2017, Oct 20]

[3] Reaction Rates [Online]. Available from: http://slideplayer.com/slide/10788240/ [2017, Oct 21]

[4] The effect of catalysts on reaction rates [Online]. Available from: http://www.chemguide.co.uk/physical/basicrates/catalyst.html [2017, Oct 21]

[5] Describe the effect of a catalyst on a chemical reaction / Maxwell-Bolztmann curves [Online]. Available from: https://www.youtube.com/watch?v=wDkii633T9Q [2017, Oct 20]

[6] Farnetti, E., Monte, R.D., and Kašpar, J. HOMOGENEOUS AND HETEROGENEOUS CATALYSIS in *INORGANIC AND BIO-INORGANIC CHEMISTRY*.

[7] Freitas, E.F., Paiva, M.F., Dias, S.C.L., and Dias, J.A. Generation and characterization of catalytically active sites of heteropolyacids on zeolite Y for liquid-phase esterification. Catalysis Today 289(Supplement C) (2017): 70-77.

[8] Zhu, Y., et al. Highly chemoselective esterification for the synthesis of monobutyl itaconate catalyzed by hierarchical porous zeolites. Journal of Catalysis 299(Supplement C) (2013): 20-29.

[9] Mishra, S., Balyan, S., Pant, K.K., and Haider, M.A. Non-oxidative conversion of methane into higher hydrocarbons over Mo/MCM-22 catalyst. Journal of Chemical Sciences (2017).

[10] Yusoff, M.H.M. and Abdullah, A.Z. Catalytic behavior of sulfated zirconia supported on SBA-15 as catalyst in selective glycerol esterification with palmitic acid to monopalmitin. Journal of the Taiwan Institute of Chemical Engineers 60 (2016): 199-204.

[11] Käldström, M., Kumar, N., and Murzin, D.Y. Valorization of cellulose over metal supported mesoporous materials. Catalysis Today 167(1) (2011): 91-95.

[12] Díaz, I., Márquez-Alvarez, C., Mohino, F., Pérez-Pariente, J.n., and Sastre, E. Combined Alkyl and Sulfonic Acid Functionalization of MCM-41-Type Silica. Journal of Catalysis 193(2) (2000): 295-302.

[13] Zhao, Y., Zhang, X., Song, X., and Liu, F. Highly Active and Recyclable Mesoporous Molecular Sieves CaO(SrO,BaO)/SBA-15 with Base Sites as Heterogeneous Catalysts for Methanolysis of Polycarbonate. Catalysis Letters (2017).

[14] Guldhe, A., Singh, P., Ansari, F.A., Singh, B., and Bux, F. Biodiesel synthesis from microalgal lipids using tungstated zirconia as a heterogeneous acid catalyst and its comparison with homogeneous acid and enzyme catalysts. Fuel 187(Supplement C) (2017): 180-188.

[15] Ispir, E., Sahin, E., Ikiz, M., and Aktas, A. Comparative transfer hydrogenation performance of homogeneous and heterogeneous ruthenium (II) catalysts derived from a Schiff base ligand. Journal of Organometallic Chemistry 830(Supplement C) (2017): 188-195.

[16] ACS Symposium: Finding Alternatives to Critical Materials in Photovoltaics and Catalysis from an Academic and Industrial Perspective [Online]. Available from: https://www.slideshare.net/ChEnected/acs-symposium-finding-alternatives-to-critical-materials-in-photovoltaics-and-catalysis-from-an-industrial-perspective [2017, Oct 20]

[17] Heterogeneous catalysis [Online]. Available from: http://slideplayer.com/slide/8482317/ [2017, Oct 20]

[18] Wan, Z., Li, G.K., Wang, C., Yang, H., and Zhang, D. Relating coke formation and characteristics to deactivation of ZSM-5 zeolite in methanol to gasoline conversion. Applied Catalysis A: General 549(Supplement C) (2018): 141-151.

[19] Maghsoudi, H. and Aidani, A. Experimental adsorption isotherms of CO2 and CH4 on STT zeolite: comparison with high- and pure-silica zeolites. Adsorption (2017).

[20] Wu, W., Guo, W., Ji, Z., Liu, Y., Hu, X., and Liu, Z. Static and dynamic sorption study of heavy metal ions on amino-functionalized SBA-15. Journal of Dispersion Science and Technology (2017): 1-11.

[21] Owens, G.J., et al. Sol–gel based materials for biomedical applications. Progress in Materials Science 77(Supplement C) (2016): 1-79.

[22] Gibson, L.T. Mesosilica materials and organic pollutant adsorption: part A removal from air. Chemical Society Reviews 43(15) (2014): 5163-5172.

[23] Jeenpadiphat, S. Esterification of free fatty acid and oil with fatty acid content over acidic heterogeneous catalyst. Doctor of Philosophy, Nanoscience and Technology Chulalongkorn university.

[24] Szyma**ń**ski, A. Determination of Sulfonamide Residues in Food by Micellar Liquid Chromatography. Toxicology Mechanisms and Methods 18(6) (2008): 473-481.

[25] Alothman, Z. A Review: Fundamental Aspects of Silicate Mesoporous Materials. Materials 5(12) (2012): 2874-2902.

[26] Samiey, B., Cheng, C.H., and Wu, J. Organic-Inorganic Hybrid Polymers as Adsorbents for Removal of Heavy Metal Ions from Solutions: A Review. Materials (Basel) 7(2) (2014): 673-726.

[27] Zhao, D., et al. Triblock Copolymer Syntheses of Mesoporous Silica with Periodic 50 to 300 Angstrom Pores. Science 279(5350) (1998): 548.

[28] Trewyn, B.G., Nieweg, J.A., Zhao, Y., and Lin, V.S.Y. Biocompatible mesoporous silica nanoparticles with different morphologies for animal cell membrane penetration. Chemical Engineering Journal 137(1) (2008): 23-29.

[29] Hoo, P.-Y. and Abdullah, A.Z. Direct synthesis of mesoporous 12-tungstophosphoric acid SBA-15 catalyst for selective esterification of glycerol and lauric acid to monolaurate. Chemical Engineering Journal 250 (2014): 274-287.

[30] Bahrami, Z., Badiei, A., and Atyabi, F. Surface functionalization of SBA-15 nanorods for anticancer drug delivery. Chemical Engineering Research and Design 92(7) (2014): 1296-1303.

[31] Wang, S., Wang, K., Dai, C., Shi, H., and Li, J. Adsorption of Pb2+ on amino-functionalized core–shell magnetic mesoporous SBA-15 silica composite. Chemical Engineering Journal 262 (2015): 897-903.

[32] Bagheryan, Z., Raoof, J.-B., Ojani, R., and Rezaei, P. Development of a new biosensor based on functionalized SBA-15 modified screen-printed graphite electrode as a nano-reactor for Gquadruplex recognition. Talanta 119(Supplement C) (2014): 24-33.

[33] Da'na, E. and Sayari, A. Adsorption of heavy metals on amine-functionalized SBA-15 prepared by co-condensation: Applications to real water samples. Desalination 285(Supplement C) (2012): 62-67.

[34] Soler-Illia, G.J.d.A.A., Crepaldi, E.L., Grosso, D., and Sanchez, C. Block copolymer-templated mesoporous oxides. Current Opinion in Colloid & Interface Science 8(1) (2003): 109-126.

[35] Cassiers, K., et al. A Detailed Study of Thermal, Hydrothermal, and Mechanical Stabilities of a Wide Range of Surfactant Assembled Mesoporous Silicas. Vol. 14, 2002.

[36] Chiral mesoporous silica behaves as a carrier of chiral drugs [Online]. Available from: http://nanotechweb.org/cws/article/lab/42565 [2017, Oct 20]

[37] Hamdan, H., Navijanti, V., Nur, H., and Mohd Nazlan Mohd, M. Fe(III)-salen encapsulated Al-MCM-41 as a catalyst in the polymerisation of bisphenol-A. Solid State Sciences 7(2) (2005): 239-244.

[38] Blin, J.L. and Imperor-Clerc, M. Mechanism of self-assembly in the synthesis of silica mesoporous materials: in situ studies by X-ray and neutron scattering. Chemical Society Reviews 42(9) (2013): 4071-4082.

[39] Hoffmann, F., Cornelius, M., Morell, J., and Froba, M. Silica-based mesoporous organic-inorganic hybrid materials. Angew Chem Int Ed Engl 45(20) (2006): 3216-51.

[40] Bruhwiler, D. Postsynthetic functionalization of mesoporous silica. Nanoscale 2(6) (2010): 887-92.

[41] Colilla, M., González, B., and Vallet-Regí, M. Mesoporous silicananoparticles for the design of smart delivery nanodevices. Biomater. Sci. 1(2) (2013): 114-134.

[42] Csicsery, S.M. Catalysis by shape selective zeolites — science and technology. pure and applied chemistry 58(6) (1986): 841-856.

[43] Rinaldi, R. and Schüth, F. Design of solid catalysts for the conversion of biomass. Energy & Environmental Science 2(6) (2009): 610.

[44] Keggin, J.F. The Structure and Formula of 12-Phosphotungstic Acid. Proceedings of the Royal Society of London. Series A 144(851) (1934): 75.

[45] Mizuno, N. and Misono, M. Heteropolyacid catalysts. Current Opinion in Solid State and Materials Science 2(1) (1997): 84-89.

[46] Manikandan, K. and Cheralathan, K.K. Heteropoly acid supported on silicalite–1 possesing intracrystalline nanovoids prepared using biomass – an efficient and recyclable catalyst for esterification of levulinic acid. Applied Catalysis A: General 547(Supplement C) (2017): 237-247.

[47] Yu, F.-L., Wang, Q.-Y., Yuan, B., Xie, C.-X., and Yu, S.-T. Alkylation desulfurization of FCC gasoline over organic-inorganic heteropoly acid catalyst. Chemical Engineering Journal 309(Supplement C) (2017): 298-304.

[48] Zhou, L., Wang, L., Diao, Y., Yan, R., and Zhang, S. Cesium salts supported heteropoly acid for oxidation of methacrolein to methacrylic acid. Molecular Catalysis 433(Supplement C) (2017): 153-161.

[49] Mioč, U.B. and Nedić, Z.P. Keggin Structure. in Drioli, E. and Giorno, L. (eds.),Encyclopedia of Membranes, pp. 1077-1079. Berlin, Heidelberg: Springer Berlin Heidelberg, 2016.

[50] Housecroft, C.E. and Sharpe, A.G. Inorganic Chemistry ed. 2nd. Vol. 6: Prentice Hall, 2004.

[51] Keggin structure [Online]. Available from: https://en.wikipedia.org/wiki/Keggin_structure [2017, Oct 22]

[52] Mazloum-Ardakani, M., Sheikh-Mohseni, M.A., and Abdollahi-Alibeik, M. Fabrication of an electrochemical sensor based on nanostructured polyaniline doped with tungstophosphoric acid for simultaneous determination of low

concentrations of norepinephrine, acetaminophen and folic acid. Journal of Molecular Liquids 178(Supplement C) (2013): 63-69.

[53] Bajuk-Bogdanović, D., et al. 12-Tungstophosphoric acid/BEA zeolite composites – Characterization and application for pesticide removal. Materials Science and Engineering: B 225(Supplement C) (2017): 60-67.

[54] de Godói Silva, V.W., Laier, L.O., and Silva, M.J.d. Novel H3PW12O40: Catalysed Esterification Reactions of Fatty Acids at Room Temperature for Biodiesel Production. Catalysis Letters 135(3) (2010): 207-211.

[55] Patel, A. and Singh, S. A green and sustainable approach for esterification of glycerol using 12-tungstophosphoric acid anchored to different supports: Kinetics and effect of support. Fuel 118 (2014): 358-364.

[56] Castanheiro, J.E., Fonseca, I.M., Ramos, A.M., and Vital, J. Tungstophosphoric acid immobilised in SBA-15 as an efficient heterogeneous acid catalyst for the conversion of terpenes and free fatty acids. Microporous and Mesoporous Materials 249(Supplement C) (2017): 16-24.

[57] Mohan Reddy, K., Seshu Babu, N., Sai Prasad, P.S., and Lingaiah, N. Aluminium-exchanged tungstophosphoric acid: An efficient catalyst for intermolecular hydroarylation of vinyl arenes. Catalysis Communications 9(15) (2008): 2525-2531.

[58] Li, S., et al. Magnetic and Stable H 3 PW 12 O 40 -Based Core@shell Nanomaterial towards the Esterification of Oleic Acid with Methanol. Vol. 2013, 2013.

[59] Singh, S. and Patel, A. Selective Green Esterification and Oxidation of Glycerol over 12-Tungstophosphoric Acid Anchored to MCM-48. Industrial & Engineering Chemistry Research 53(38) (2014): 14592-14600.

[60] Wang, Y., Song, H., and Sun, X. Alkylation of toluene with tert-butyl alcohol over HPW-modified Hβ zeolite. Chinese Journal of Catalysis 37(12) (2016): 2134-2141.

[61] Li, S., Qi, X., and Huang, B. Synthesis of 7-hydroxy-4-methylcoumarin via the Pechmann reaction with PVP-supported phosphotungstic acid catalyst. Catalysis Today 276(Supplement C) (2016): 139-144.

[62] Pires, L.H.O., et al. Esterification of a waste produced from the palm oil industry over 12-tungstophosforic acid supported on kaolin waste and mesoporous materials. Applied Catalysis B: Environmental 160(Supplement C) (2014): 122-128.

[63] Liu, J., Liu, Y., Yang, W., Guo, H., Fang, F., and Tang, Z. Immobilization of phosphortungstic acid on amino-functionalized bimetallic Zr–La-SBA-15 and its highly catalytic performance for acetylation. Journal of Molecular Catalysis A: Chemical 393 (2014): 1-7.

[64] Xie, W. and Hu, P. Production of Structured Lipids Containing Medium-Chain Fatty Acids by Soybean Oil Acidolysis Using SBA-15-pr-NH2–HPW Catalyst in a Heterogeneous Manner. Organic Process Research & Development 20(3) (2016): 637-645.

[65] Kong, P.S., Aroua, M., and Daud, W. Catalytic esterification of bioglycerol to value-added products. Vol. 31, 2015.

[66] The mechanism for the esterification reaction [Online]. Available from: http://www.chemguide.co.uk/physical/catalysis/esterify.html [2017, Oct 28]

[67] Szela¸g, H. and Zwierzyko, W. Esterification kinetics of glycerol with fatty acids in the presence of sodium and potassium soaps. European Journal of Lipid Science and Technology 100(7) (1998): 302-307.

[68] Sánchez, N., Martínez, M., and Aracil, J. Selective Esterification of Glycerine to 1-Glycerol Monooleate. 1. Kinetic Modeling. Industrial & Engineering Chemistry Research 36(5) (1997): 1524-1528.

[69] Macierzanka, A. and Szela¸g, H. Esterification Kinetics of Glycerol with Fatty Acids in the Presence of Zinc Carboxylates: Preparation of Modified Acylglycerol Emulsifiers. Industrial & Engineering Chemistry Research 43(24) (2004): 7744-7753.

[70] Moquin, P.H.L. and Temelli, F. Production of monoolein from oleic acid and glycerol in supercritical carbon dioxide media: A kinetic approach. The Journal of Supercritical Fluids 44(1) (2008): 40-47.

[71] Wee, L.H., et al. Synthesis of Monoglycerides by Esterification of Oleic Acid with Glycerol in Heterogeneous Catalytic Process Using Tin–Organic Framework Catalyst. Catalysis Letters 143(4) (2013): 356-363.

[72] Ferreira, P., Fonseca, I.M., Ramos, A.M., Vital, J., and Castanheiro, J.E. Acetylation of glycerol over heteropolyacids supported on activated carbon. Catalysis Communications 12(7) (2011): 573-576.

[73] Lu, N., et al. Design of polyoxometallate–titania composite film (H3PW12O40/TiO2) for the degradation of an aqueous dye Rhodamine B under the simulated sunlight irradiation. Journal of Hazardous Materials 199 (2012): 1-8.

[74] Yan, X.-m., Su, G.-s., and Xiong, L. Oxidative desulfurization of diesel oil over Ag-modified mesoporous HPW/SiO2 catalyst. Journal of Fuel Chemistry and Technology 37(3) (2009): 318-323.

[75] Baroi, C. and Dalai, A.K. Esterification of free fatty acids (FFA) of Green Seed Canola (GSC) oil using H-Y zeolite supported 12-Tungstophosphoric acid (TPA). Applied Catalysis A: General 485 (2014): 99-107.

[76] Sheng, X., Kong, J., Zhou, Y., Zhang, Y., Zhang, Z., and Zhou, S. Direct synthesis, characterization and catalytic application of SBA-15 mesoporous silica with heteropolyacid incorporated into their framework. Microporous and Mesoporous Materials 187 (2014): 7-13.

[77] Tropecêlo, A.I., Casimiro, M.H., Fonseca, I.M., Ramos, A.M., Vital, J., and Castanheiro, J.E. Esterification of free fatty acids to biodiesel over heteropolyacids immobilized on mesoporous silica. Applied Catalysis A: General 390(1–2) (2010): 183-189.

[78] Calleja, G., Sanz, R., Arencibia, A., and Sanz-Pérez, E.S. Influence of Drying Conditions on Amine-Functionalized SBA-15 as Adsorbent of CO2. Topics in Catalysis 54(1) (2011): 135-145.

[79] Hu, W., Zhang, Y., Huang, Y., Wang, J., Gao, J., and Xu, J. Selective esterification of glycerol with acetic acid to diacetin using antimony pentoxide as reusable catalyst. Journal of Energy Chemistry 24(5) (2015): 632-636.

[80] Tamayo, J.J., Ladero, M., Santos, V.E., and García-Ochoa, F. Esterification of benzoic acid and glycerol to α-monobenzoate glycerol in solventless media using an industrial free Candida antarctica lipase B. Process Biochemistry 47(2) (2012): 243-250.

[81] Molinero, L., Ladero, M., Tamayo, J.J., and García-Ochoa, F. Homogeneous catalytic esterification of glycerol with cinnamic and methoxycinnamic acids to cinnamate glycerides in solventless medium: Kinetic modeling. Chemical Engineering Journal 247 (2014): 174-182.

[82] Sánchez, D.A., Tonetto, G.M., and Ferreira, M.L. Enzymatic synthesis of 1,3-dicaproyglycerol by esterification of glycerol with capric acid in an organic solvent system. Journal of Molecular Catalysis B: Enzymatic 100 (2014): 7-18.

[83] Kotwal, M., Deshpande, S.S., and Srinivas, D. Esterification of fatty acids with glycerol over Fe–Zn double-metal cyanide catalyst. Catalysis Communications 12(14) (2011): 1302-1306.

[84] Freitas, L., Paula, A.V., dos Santos, J.C., Zanin, G.M., and de Castro, H.F. Enzymatic synthesis of monoglycerides by esterification reaction using Penicillium camembertii lipase immobilized on epoxy SiO2-PVA composite. Journal of Molecular Catalysis B: Enzymatic 65(1–4) (2010): 87-90.

[85] An, S., Sun, Y., Song, D., Zhang, Q., Guo, Y., and Shang, Q. Arenesulfonic acid-functionalized alkyl-bridged organosilica hollow nanospheres for selective esterification of glycerol with lauric acid to glycerol mono- and dilaurate. Journal of Catalysis 342 (2016): 40-54.

[86] Hamerski, F. and Corazza, M.L. LDH-catalyzed esterification of lauric acid with glycerol in solvent-free system. Applied Catalysis A: General 475 (2014): 242-248.

[87] Singh, D., Patidar, P., Ganesh, A., and Mahajani, S. Esterification of Oleic Acid with Glycerol in the Presence of Supported Zinc Oxide as Catalyst. Industrial & Engineering Chemistry Research 52(42) (2013): 14776-14786.

[88] Zhang, Z., Zhang, F., Zhu, Q., Zhao, W., Ma, B., and Ding, Y. Magnetically separable polyoxometalate catalyst for the oxidation of dibenzothiophene with H2O2. Journal of Colloid and Interface Science 360(1) (2011): 189-194.

[89] Mbaraka, I.K., Radu, D.R., Lin, V.S.Y., and Shanks, B.H. Organosulfonic acid-functionalized mesoporous silicas for the esterification of fatty acid. Journal of Catalysis 219(2) (2003): 329-336.

[90] Alsalme, A., Kozhevnikova, E.F., and Kozhevnikov, I.V. Heteropoly acids as catalysts for liquid-phase esterification and transesterification. Applied Catalysis A: General 349(1–2) (2008): 170-176.

[91] Hermida, L., Abdullah, A.Z., and Mohamed, A.R. Synthesis of monoglyceride through glycerol esterification with lauric acid over propyl sulfonic acid post-synthesis functionalized SBA-15 mesoporous catalyst. Chemical Engineering Journal 174(2–3) (2011): 668-676.

[92] Karaki, M., Karout, A., Toufaily, J., Rataboul, F., Essayem, N., and Lebeau, B. Synthesis and characterization of acidic ordered mesoporous organosilica SBA-15: Application to the hydrolysis of cellobiose and insight into the stability of the acidic functions. Journal of Catalysis 305 (2013): 204-216.

[93] Zhu, Y., Li, H., Zheng, Q., Xu, J., and Li, X. Amine-functionalized SBA-15 with uniform morphology and well-defined mesostructure for highly sensitive chemosensors to detect formaldehyde vapor. Langmuir 28(20) (2012): 7843-50.

[94] Chen, Y., Cao, Y., Suo, Y., Zheng, G.-P., Guan, X.-X., and Zheng, X.-C. Mesoporous solid acid catalysts of 12-tungstosilicic acid anchored to SBA-15: Characterization and catalytic properties for esterification of oleic acid with methanol. Journal of the Taiwan Institute of Chemical Engineers 51 (2015): 186-192.

[95] Dong, B.-B., Zhang, B.-B., Wu, H.-Y., Chen, X., Zhang, K., and Zheng, X.-C. Synthesis, characterization and catalytic evaluation of SBA-15 supported 12-tungstophosphoric acid mesoporous materials in the oxidation of benzaldehyde to benzoic acid. Materials Research Bulletin 48(7) (2013): 2491-2496.

[96] Geng, T., Li, Q., Jiang, Y., and Wang, W. Esterification of Stearic Acid with Triethanolamine over Zirconium Sulfate Supported on SBA-15 Mesoporous Molecular Sieve. Journal of Surfactants and Detergents 14(1) (2011): 15-22.

[97] Khayoon, M.S. and Hameed, B.H. Synthesis of hybrid SBA-15 functionalized with molybdophosphoric acid as efficient catalyst for glycerol esterification to fuel additives. Applied Catalysis A: General 433–434 (2012): 152-161.

[98] Eldik, R.V. K. A. Connors: Chemical Kinetics: The Study of Reaction Rates in Solution, VCH Verlagsgesellschaft Weinheim, New York, ISBN 3-527-28037-5, 480 Seiten, Preis: DM 168,–. Berichte der Bunsengesellschaft für physikalische Chemie 95(9) (1991): 1160-1160.

[99] Hamerski, F., Prado, M.A., da Silva, V.R., Voll, F.A.P., and Corazza, M.L. Kinetics of layered double hydroxide catalyzed esterification of fatty acids with glycerol. Reaction Kinetics, Mechanisms and Catalysis 117(1) (2016): 253-268.

[100] Konwar, L.J., Mäki-Arvela, P., Kumar, N., Mikkola, J.-P., Sarma, A.K., and Deka, D. Selective esterification of fatty acids with glycerol to monoglycerides over –SO3H functionalized carbon catalysts. Reaction Kinetics, Mechanisms and Catalysis 119(1) (2016): 121-138.

[101] Database of Zeolite Structures [Online]. Available from: http://asia.iza-structure.org/IZA-SC/framework.php?STC=BEA [2017, Oct 16]

[102] Database of Zeolite Structures [Online]. Available from: http://asia.iza-structure.org/IZA-SC/framework.php?STC=MFI [2016, Oct 16]

[103] Amberlyst® 15 hydrogen form [Online]. Available from: http://www.sigmaaldrich.com/catalog/product/aldrich/216399?lang=en&region=SG&gclid=Cj0KCQjwsZHPBRClARIsAC-

VMPAOGNZasjEeGt_VfkBqHIBm22NIVx11vOHLXPOjdmKlOtsE8LeT2wOaAhaOEALw_wcB [2017, Oct 16]

[104] First-Order Reactions [Online]. Available from: https://chem.libretexts.org/Core/Physical_and_Theoretical_Chemistry/Kinetics/Reaction_Rates/First-Order_Reactions

APPENDIX

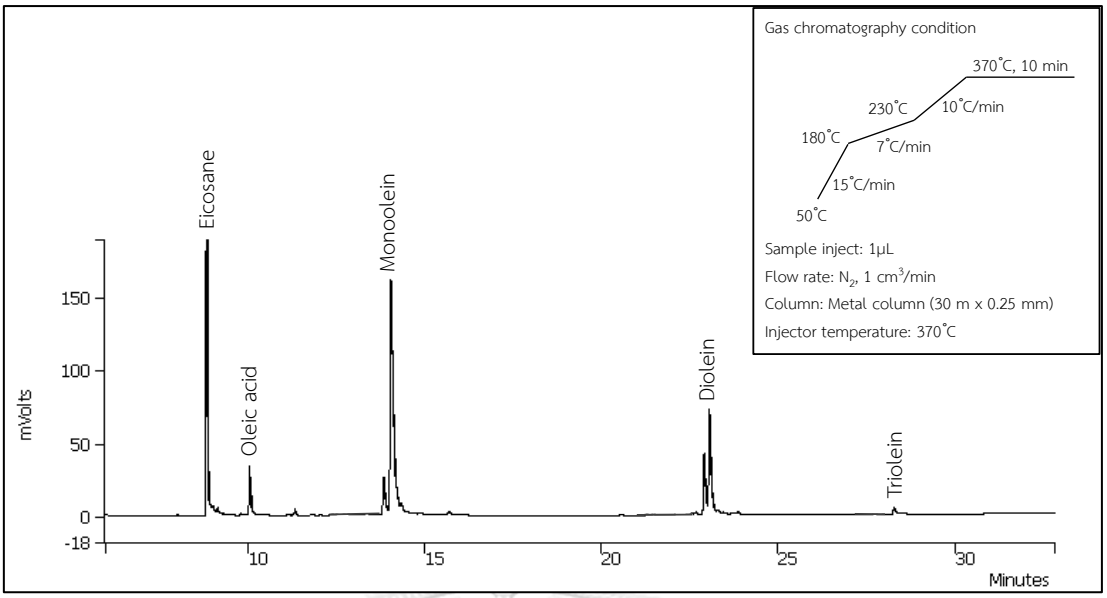

Figure A-1 A gas chromatogram illustrated the sample analysis of glyceride products from esterification of glycerol with oleic acid using eicosane as the internal standard.

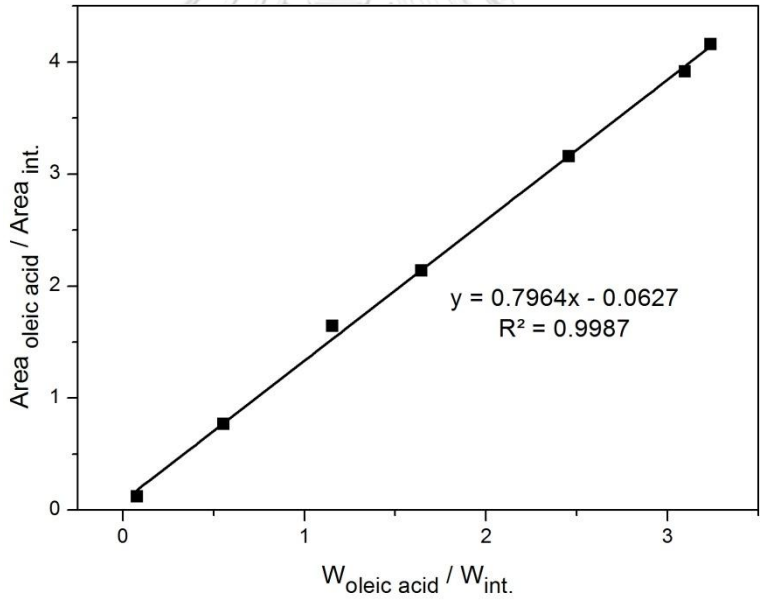

Figure A-2 Calibration curve of oleic acid analyzed by GC using eicosane as the internal standard.

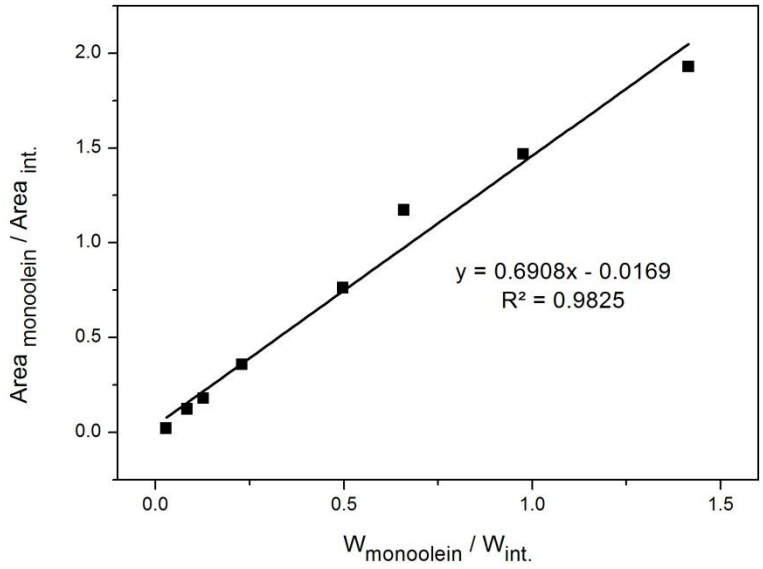

Figure A-3 Calibration curve of monoolein analyzed by GC using eicosane as the internal standard.

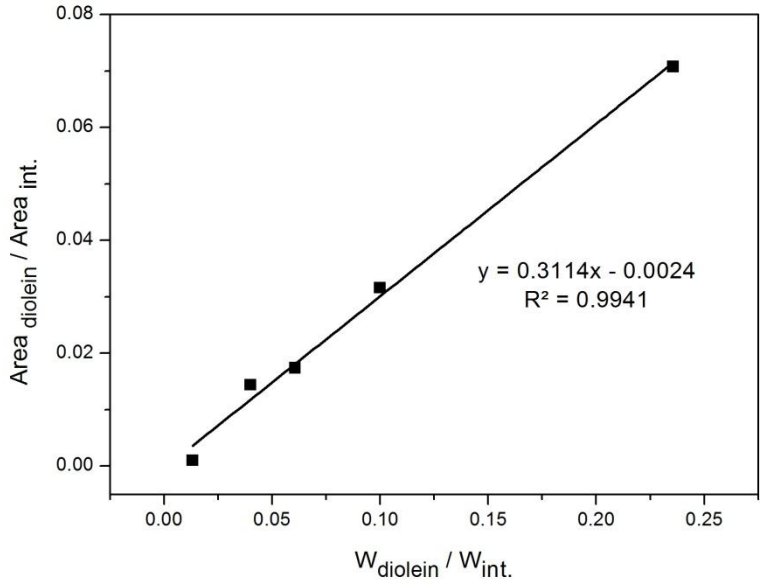

Figure A-4 Calibration curve of diolein analyzed by GC using eicosane as the internal standard.

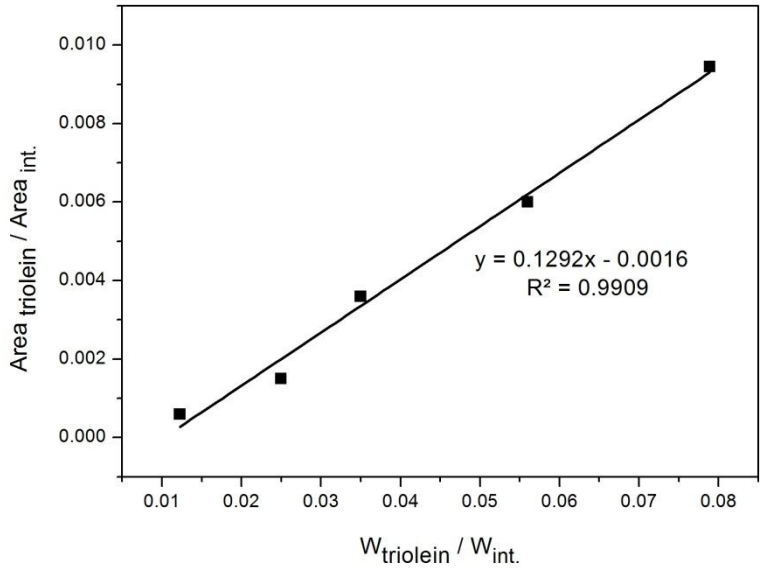

Figure A-5 Calibration curve of triolein analyzed by GC using eicosane as the internal standard.

VITA

Miss Kullatida Ratchadapiban was born on February 3, 1992 in Hatyai, Thailand. She graduated with Bachelor's Degree in Chemistry from Faculty of Science, Kasetsart University in 2014. In addition, she continued her study in Inorganic chemistry, Faculty of Science, Chulalongkorn university in 2014 and she has completed her study in a Master's Degree in Chemistry in 2017. She presented her research in Pure and Applied Chemistry International Conference (PACCON 2017) in the topic of "Monoolein production from esterification of glycerol with oleic acid using tungstophosphoric acid supported on functionalized SBA-15".

Her present address is 5, Mandarin, Airport road, Hatyai, Songkhla, Thailand 90110. E-mail address: r.kullatida@hotmail.com